TUNABLE 10 MICRON LASER, AN INTEGRATED OPTICS APPROACH TO INFRARED GAS LASERS

D. B. Anderson, et al

Rockwell International Corporation

Prepared for:

Office of Naval Research

27 June 1973

C72-650.16/501

SECOND SEMI-ANNUAL TECHNICAL REPORT

TUNABLE 10 MICRON LASER
AN INTEGRATED OPTICS APPROACH TO INFRARED GAS LASERS

By

D. B. Anderson
K. R. August
J. O. McMullen
R. Shubert
R. L. Davis
L. A. Jenkins

June 27, 1973

Prepared for the Director, Naval Research Laboratory
Contract N00014-72-C-0505

1 June 1972 to 31 December 1973 - $99,306
Sponsored by
Advanced Research Projects Agency
ARPA Order #1806, Amendment #9, Dated November 15, 1972
Program Code 3E90

Electronics Research Division, Electronics Group
Rockwell International
3370 Miraloma; Anaheim, California 92803

SECOND SEMI-ANNUAL TECHNICAL REPORT

C72-650.16/501

TUNABLE 10 MICRON LASER:
AN INTEGRATED OPTICS APPROACH TO INFRARED GAS LASERS

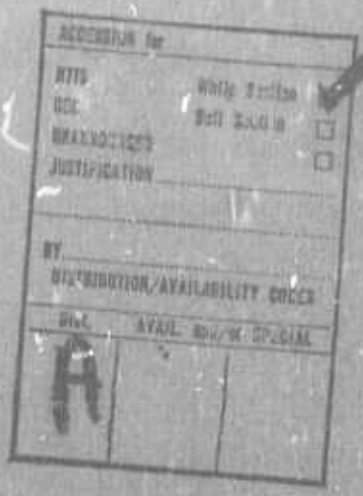

by

D. B. Anderson
Program Manager
(714) 832-1889

R. R. August
J. D. McMullen
R. Shubert
R. L. Davis
L. A. Jankins

June 27, 1973

Prepared for the Director, Naval Research Laboratory
Contract N00014-72-C-0505

1 June 1972 to 31 December 1973 - $99,306
Sponsored by
Advanced Research Projects Agency
ARPA Order #1806, Amendment #9, dated 11-15-72
Program Code 3E90

Electronics Research Division, Electronics Group
Rockwell International
3370 Miraloma; Anaheim, California 92803

E. REFERENCES

1. J. A. Stratton, Electromagnetic Theory, (McGraw-Hill, New York, 1941), Ch. IX.

2. E. A. J. Marcatili and R. A. Schmeltzer, "Hollow Metallic and Dielectric Waveguides for Long Distance Optical Transmission and Lasers," Bell Sys. Tech. J., 1783 (1964).

3. A. Reisinger, "Characteristics of Optical Guided Modes in Lossy Waveguides," Applied Optics, 12, 1015 (1973).

4. R. L. Abrams and W. B. Bridges "Characteristics of Sealed-off Waveguide CO_2 Lasers," to be published.

5. W. G. Spitzer and D. A. Kleinman, "Infrared Lattice Bands of Quartz," Phys. Rev., 121, 1324 (1961).

6. E. Loh, "Optical Phonons in BeO Crystals," Phys. Rev., 166, 673 (1968).

7. A. S. Barker, Jr., "Infrared Lattice Vibrations and Dielectric Dispersion in Corundum," Phys. Rev., 132, 1474 (1963).

8. S. P. S. Porto, "Raman Effect of Corundum," J. Chem Phys., 47, 1009 (1967).

UNCLASSIFIED

Security Classification

DOCUMENT CONTROL DATA - R & D

(Security classification of title, body of abstract and indexing annotation must be entered when the overall report is classified)

1 ORIGINATING ACTIVITY (Corporate author)

ROCKWELL INTERNATIONAL CORPORATION

2a. REPORT SECURITY CLASSIFICATION

Unclassified

2b. GROUP

3 REPORT TITLE

TUNABLE 10 MICRON LASER, AN INTEGRATED OPTICS APPROACH TO INFRARED GAS LASERS

4 DESCRIPTIVE NOTES (Type of report and inclusive dates)

Second Semi-Annual Technical Report, June 1, 1972 - December 31, 1973

5 AUTHOR(S) (First name, middle initial, last name)

D. B. Anderson, J. D. McMullen, R. L. Davis, R. R. August, R. Shubert, L. A. Jenkins

6 REPORT DATE	7a. TOTAL NO. OF PAGES	7b. NO. OF REFS
June 27, 1973	~~42 + 18A~~ 66	27 + 8A

8a. CONTRACT OR GRANT NO.	9a. ORIGINATOR'S REPORT NUMBER(S)
Contract N00014-72-C-0505	C72-650.16/501
b. PROJECT NO. ARPA Order No. 1806, Amendment #9 dtd November 15, 1972	9b. OTHER REPORT NO(S) (Any other numbers that may be assigned this report)
c.	
d.	

10 DISTRIBUTION STATEMENT

Distribution of this document is unlimited.

11 SUPPLEMENTARY NOTES	12. SPONSORING MILITARY ACTIVITY
Prepared for Office of Naval Research	Sponsored by Advanced Research Projects Agency

13 ABSTRACT The further development of a tunable CO_2 laser employing an integrated optics approach to its construction is delineated herein. The apposite laser design parameters emphasize application as a local oscillator for a tunable optical heterodyne receiver. The integrated optics approach employs a nonuniform distributed iterative passive waveguide in close proximity to a planar active gas waveguide to form the resonant circuit. Backward wave Bragg diffraction is employed between the active gas and the passive feedback waveguide. Transverse gas flow and transverse excitation are considered as opposed to the longitudinal configuration of a capillary waveguide laser. The incorporation of a traveling surface elastic wave (Rayleigh) collinear and within the passive feedback waveguide to alter the dispersion is the approach considered to achieve the wide unambiguous tuning range. Major accomplishments during the second reporting period include: 1) Successful demonstration of a hollow planar waveguide CO_2 laser using transverse flow, transverse excitation, and miniature waveguide Fabry-Perot reflectors, 2) Improved understanding and capability to produce continuous uniform plasma discharges at elevated pressure in constrictions imposed by the waveguide, 3) The analysis of waveguide wall materials considering the influence of infrared active phonons (Appendix A), and 4) The development of a photolithographic process to produce a long continuous diffraction grating for use as the distributed feedback with sufficiently deep undulations to affect high reflectivity of the backward wave. Correspondingly, problems encountered relating to the production of a continuous uniform transverse plasma discharge at the required high pressures in constricted waveguide sections are divergent from design considerations essential for achievement of a wide unambiguous tuning range. Determination of the trade-offs while sustaining a laser operation will continue to be a dominant ~~experimentally determined design constraint.~~

DD FORM 1 NOV 65 1473

1a

UNCLASSIFIED

Security Classification

14 KEY WORDS	LINK A		LINK B		LINK C	
	ROLE	WT	ROLE	WT	ROLE	WT
CO_2 GAS LASER						
INTEGRATED OPTICS						
DISTRIBUTED FEEDBACK						
BACKWARD WAVE BRAGG DIFFRACTION COUPLER						
CAPILLARY WAVEGUIDE LASER						
PLANAR WAVEGUIDE LASER						
PLANAR PLASMA DISCHARGE						
TRANSVERSE EXCITATION						

SUMMARY

The further development of a tunable CO_2 laser employing an integrated optics approach to its construction is delineated herein. The apposite laser design parameters emphasize application as a local oscillator for a tunable optical heterodyne receiver.

The integrated optics approach employs a nonuniform distributed iterative passive waveguide in close proximity to a planar active gas waveguide to form the resonant circuit. Backward wave Bragg diffraction is employed between the active gas and the passive feedback waveguide. Transverse gas flow and transverse excitation are considered as opposed to the longitudinal configuration of a capillary waveguide laser. The incorporation of a traveling surface elastic wave (Rayleigh) collinear and within the passive feedback waveguide to alter the dispersion is the approach considered to achieve the wide unambiguous tuning range.

Major accomplishments during the second reporting period include:

1. Successful demonstration of a hollow planar waveguide CO_2 laser using transverse flow, transverse excitation, and miniature waveguide Fabry-Perot reflectors,

2. Improved understanding and capability to produce continuous uniform plasma discharges at elevated pressure in constrictions imposed by the waveguide,

3. The analysis of waveguide wall materials considering the influence of infrared active phonons (Appendix A), and

4. The development of a photolithographic process to produce a long continuous diffraction grating for use as the distributed feedback with sufficiently deep undulations to affect high reflectivity of the backward wave.

Correspondingly, problems encountered relating to the production of a continuous uniform transverse plasma discharge at the required high pressures in constricted waveguide sections are divergent from design considerations essential for achievement of a wide unambiguous tuning range. Determination of the trade-offs while sustaining a laser operation will continue to be a dominant experimentally determined design constraint.

TABLE OF CONTENTS

TABLE OF CONTENTS, CONTINUED

I. INTRODUCTION

A. PROGRAM OBJECTIVE

The characteristics of a CO_2 laser are regarded as an excellent source for active sensors because: (1) it is capable of high power output realized efficiently, (2) this emission band is in a superior atmospheric window which is least affected meteorologically, and (3) the associated tolerances are commensurate with high gain apertures.

The superheterodyne receiver provides the ultimate sensitivity in the far infrared. Wide band performance is required for high range resolution while frequency stability is required for high spatial resolution derived from transverse Doppler signal processing. The presence of a Doppler offset requires either wide band photodetection accepting the noise degradation due to the excess bandwidth or a tunable local oscillator with corresponding offset for tracking the Doppler. The received base-band signal with Doppler extends into the microwave region. However, photodetector response is severely limited in the microwave region. Use of a wide range continuous tunable local oscillator will relieve the severe fast response requirements of the photodetector.

Typical laboratory CO_2 lasers employ comparatively long Fabry-Perot resonators to achieve high power output. However, the close proximity of the longitudinal Fabry-Perot modes severely limit the tuning range. Current engineering practices to increase the tuning range by reducing the Fabry-Perot length generally lead to a trade-off with power output. Further, these CO_2 lasers operate at a pressure which produces a collision-broadened linewidth comparable to the longitudinal mode period, thus producing a single emmission line. A substantial increase of pressure approaching 1/2 atmosphere is essential to collision-broaden the emission linewidth sufficiently to accommodate the tuning range commensurate with the Doppler offset, and in turn, the Fabry-Perot length must be severely limited to achieve a wide, unambiguous tuning range.

An effort to further develop a tunable 10 micron laser for application as a heterodyne local oscillator and to provide a sufficiently wide unambiguous tuning range is delineated in this report. The approach being developed has its roots in the capillary waveguide laser art.[1-9] However, it is unique because it employs a planar configuration compatible with the processes developed for electronic integrated circuits.

The integrated optics approach to the tunable CO_2 laser employs a distributed iterative waveguide in close proximity to the active gas to form the resonant circuit. Bragg backward wave diffraction coupling is employed between the active gas waveguide and the passive feedback waveguide. Transverse gas flow and transverse dispersed excitation are considered as opposed to the longitudinal configuration of a capillary waveguide laser. The incorporation of a traveling surface elastic (Rayleigh) wave collinear and within the passive feedback waveguide to alter the dispersion is the approach considered to achieve the wide unambiguous tuning range.

B. STATUS

The initial effort documented in the First Interim Technical Report C72-650.10/501, dated February 26, 1973,[10] presents an analysis of the characteristics of nonuniform distributed feedback laser ring resonant circuits employing a coupled mode approach. One important virtue of the distributed hetero-feedback structure analyzed is the provision for design-control of the laser longitudinal mode spectrum to accommodate the requirements for a wide tuning range.[11-12] The photolithographic production of the required distributed feedback grating was not sufficiently developed to produce efficient backward wave reflections. Further, because the active gas gain must exceed the coupling, reflection and feedback waveguide lossed, it was deemed essential to verify the increased gain due to the close proximity of the waveguide walls.[3,13] This was done by extending the capillary waveguide laser art, using a 0.6 mm diameter bore. The production of a continuous uniform transverse plasma discharge at the required high

pressures in the thin planar active gas waveguide was identified as a serious problem. Both DC and RF-excitation yielded concentrated arcs in the thin waveguide section. The thin plasma discharge chamber waveguide differs drastically from that of the large chambers employed for transverse excited atmospheric CO_2 laser designs which operate only in a pulse mode.[9]

This Second Semi-Annual Technical Report delineates the results of two efforts: (1) a Rockwell International funded investigation of a general fundamental nature pertaining to continuous uniform plasma discharges within a thin constricted chamber, and (2) the continuing follow-on effort on behalf of this ARPA/ONR contract. Two fundamental technical problems have received the major attention during this reporting period. They are: (1) the production of a uniform continuous plasma discharge at elevated pressure in the constriction imposed by the waveguide, and (2) the photolithographic production of a long continuous diffraction grating with sufficiently deep undulations. Continuous laser operation in a hollow planar waveguide section using transverse flow, transverse excitation, and miniature waveguide Fabry-Perot reflectors was successfully demonstrated. The immediate on-going effort is concentrated upon further improvement of the discharge characteristics and the combining of the active waveguide together with the distributed feedback structure.

The planar waveguide CO_2 laser has employed fused silica and polycrystalline BeO super- and substrate materials for the experiments. The optical properties of the super- and substrate dielectric contribute substantially to the losses in the waveguide, particularly when the frequency employed is near the peak in the absorption and reflectivity for the wall material. An analysis of these waveguide wall losses is included as Appendix A, entitled, "Optical Dielectric Waveguides--Influence of Infrared Active Phonons in the Wall Dielectric."

Using the closed-form solution for the dispersion characteristics of a circular-hollow (capillary) waveguide, the frequency dependence of the attenuation of the TE_{01} mode was calculated for quartz (SiO_2),

BeO, and sapphire (Al_2O_3) wall materials. The mode attenuation coefficient for BeO walls was smaller than for quartz and sapphire walls by a factor of 10 to 40 over the range of free-space wavelengths of the CO_2 laser between 9.2 and 10.6 microns. The lower loss of the BeO waveguide mode is attributed to the strong peak in reflectivity of the dielectric between TO and LO phonon frequencies. From the frequency dependence of the mode attenuation, criteria were developed for selecting wall dielectrics which give minimum waveguide losses at any desired frequency of operation.

II. TECHNICAL DISCUSSION

A. TUNABLE CO_2 LASER, AN INTEGRATED OPTICS APPROACH

The design approach delineated in the initial Interim Technical Report (C72-650.10/501) is being implemented and investigated further. Because the approach differs radically from that of current practices relating to the CO_2 capillary laser, this section will briefly outline this integrated optics approach for the tunable CO_2 laser.

The design emphasizes a planar active waveguide structure arranged to provide transverse flow and transverse excitation of the CO_2: N_2: He gas mixture instead of the collinear confinement by the capillary. The active waveguide containing the CO_2 plasma discharge is paralleled with a passive feedback waveguide wherein both waveguides are coupled via backward wave Bragg diffraction gratings to form a ring resonant circuit (no area). The transverse and longitudinal cross sections as conceived are illustrated in Figure 1. The structure illustrated may be fabricated entirely with an expanded planar processing technology arising from the electronic integrated circuit art.

At this point in the program only certain facets have been developed while others are contingent upon further investigation. For example, transverse excitation is illustrated whereas the problems encountered as related herein may dictate application of a collinear longitudinal excitation to achieve stability. The use of a traveling surface elastic wave collinear and within the passive feedback wave is considered to alter the dispersion, however, it may be prudent to employ the electro-optic effect.

Referring to the transverse cross section, the active waveguide containing the CO_2 plasma and contributing to the gain is a rectangular cross section 100 μ in height and 3000 μ in width. The superstrate and substrate walls together with diffraction by the feedback grating provides containment within this cross section. A 9 cm active waveguide

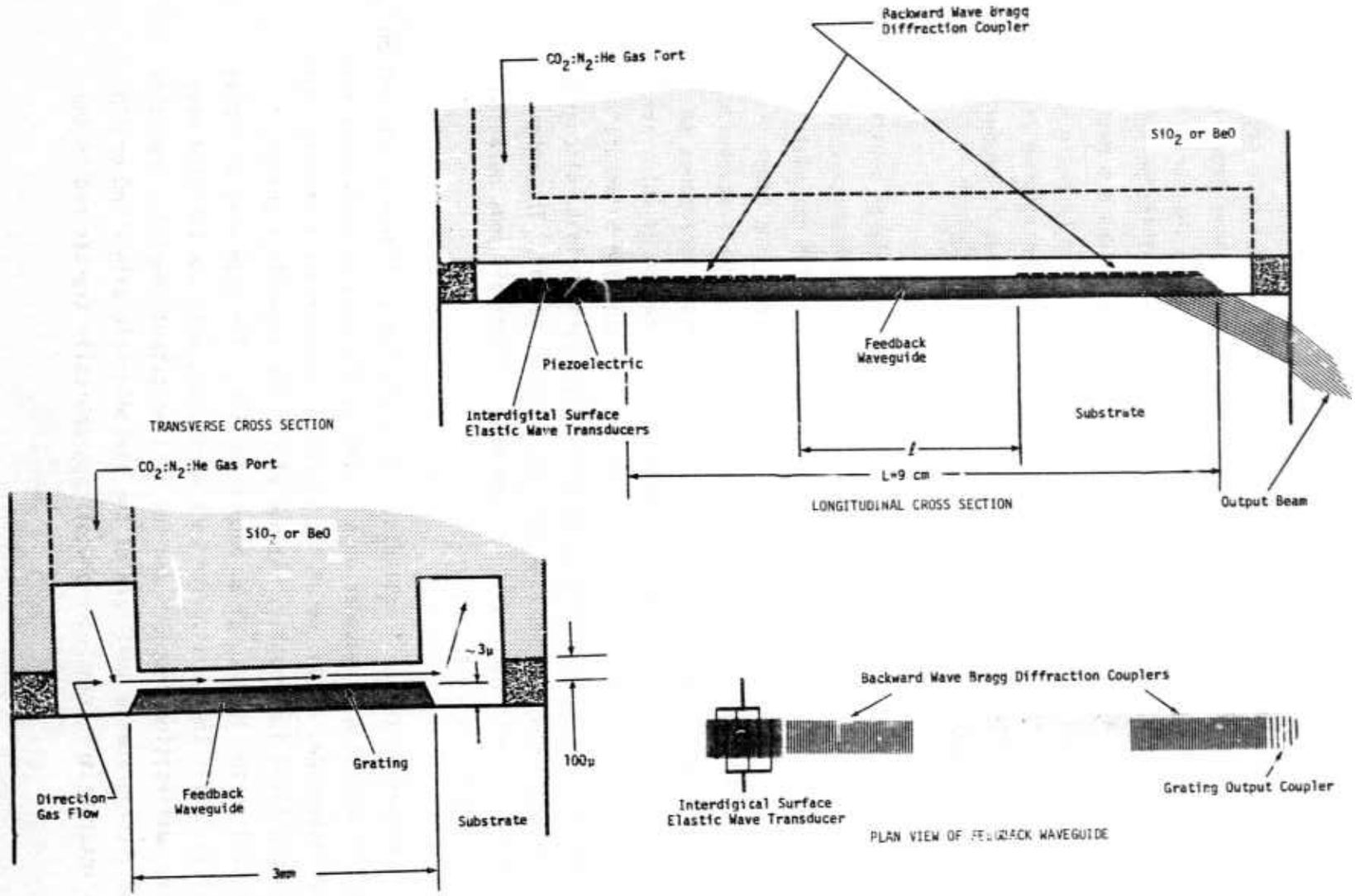

Figure 1. Integrated Optics Approach to the CO_2 Laser--Transverse Longitudinal Plan Cross Sections

length is considered adequate to overcome the losses when the gain is enhanced by the close proximity of the super- and substrate walls. The thin film waveguide will employ As_2Se_3 with a transverse cross section of 3 μ thick and 3000 μ width. The backward wave Bragg diffraction couplers are formed by direct ion milling on the surface of the feedback waveguide. The grating and control of its period are formed by a holographic technique. Deep undulations are required for the grating to affect the high reflectivity of the backward wave. Further analytical characteristics of this form of distributed feedback and a delineation of the photolithographic process to produce the grating are included in the later sections.

The laser is composed of two parallel adjacent planar substrates. The upper section contains the CO_2: N_2: He gas ports connected to two parallel chemically-etched channels serving as the gas distribution manifold on each side of the active waveguide. The lower section enclosing the gas manifold contains the passive feedback waveguide with backward wave Bragg diffraction couplers. Various approaches to transverse excitation have been employed, the results of which are more fully delineated in a later section. The spacing between the super- and substrate controls the active waveguide height, discharge characteristics, and the backward wave grating period. The interrelation of these parameters is currently a trade-off consideration affecting the laser tunability.

Referring to the longitudinal cross section of Figure 1, the hollow active waveguide is bounded on one side by the passive dielectric feedback waveguide. Each end of the assembly incorporates a backward wave Bragg diffraction coupler. At one end of the assembly a change of grating period is used as an output coupler. The plan view of Figure 1 illustrates the passive feedback waveguide, with the backward wave Bragg diffraction couplers and the grating output coupler. The other end incorporates a small pad of the piezoelectric either ZnO or AlN. An interdigital transducer photolithographically transferred to the

piezoelectric substrate is illustrated to launch the surface elastic wave. The surface elastic wave period (frequency) controls the dispersion of a passive feedback waveguide and thus will tune the laser.

Both fused silica and polycrystalline BeO are currently employed as super- and substrates. Beryllium oxide is preferred as a superstrate because of its high thermal conductivity and its preferred infrared phonon spectrum (see Appendix A), and thus lower waveguide wall losses. The substrate material must be transparent at ten microns if the output is to be taken via a grating through the substrate. Several choices are available. They include: single crystal NaF, BaF_2, ZnS, GaAs, CdTe, and polycrystalline ZnS. Successful depositions of Te and As_2Se_3 have been performed on these substrates. Consideration of Te is merited because it exhibits the highest elasto-optic coefficient. However, it is plagued by excess absorption and low damage threshold. Arsenic tri-selenide exhibits the next highest elasto-optic coefficient and simultaneously is obtainable with absorption coefficient of $0.005cm^{-1}$.

The design of the active CO_2 waveguide volume is currently set as 100x3000 μ with a length of 10 cm although the successful operation in a planar configuration employed a height of 500 μ. Using a conservative estimate of the volumetric power density of 10 W/cm^3, the expected laser output should be approximately 300 mW. If additional power is required, the waveguide width may be increased. The waveguide length could also be increased to achieve additional gain and power output, however, at the expense of limiting the longitudinal mode spectrum period and the maximum tuning range.

A crucial feature in the design for wide range tuning is the appropriate control of the longitudinal mode spectrum, in order that a single unambiguous emission line is generated for use in optical heterodyning. The longitudinal mode spectrum of this integrated CO_2 laser design containing an active waveguide coupled with a passive feedback waveguide differs from that of conventional Fabry-Perot resonators. The longitudinal mode period is C/2L. To provide for tuning out to 1.5

GHz requires the length to be reduced such that marginal power output may be available.

For a continuous distributed feedback waveguide laser continuous circulation occurs, the gain of which determines the longitudinal mode spectrum while the grating period becomes the dominant frequency determining parameter.[14] The grating, however, also couples the various propagating transverse mode orders together.[15] When a separate dielectric feedback waveguide is provided, and a discontinuous grating is employed, as in this program, the longitudinal mode period may be increased beyond C/2L. In this case, the spectral width is critically dependent upon the active gain and the magnitude of the perturbing feedback circuit. The backward wave Bragg diffraction coupler location in the ring perimeter is offset. This is due to the use of a dielectric feedback waveguide over the longer portion of the ring. The asymmetry[16] thus introduced and the dispersion of the waveguide and the frequency selectivity of the contradirectional couplers all enter into control of the longitudinal mode spectrum.

Tuning of the integrated laser can be achieved by employing a traveling or standing surface elastic wave propagating through the feedback waveguide. The dispersion of planar dielectric waveguide used in the feedback circuit containing the surface elastic wave as a periodic perturbation is illustrated in Figure 2. It shows a Brillouin diagram for planar dielectric waveguide. The modes not identified are TE_0TM_0 TE_1TM_1TE . . . . . The dispersion of the planar dielectric waveguide is confined between free-space (c) and the phase velocity within the bulk dielectric (refractive index). The effect of the periodic perturbation as the Bragg frequency is noted as a stop band. This is the condition for the backward wave or contradirectional coupler. At this frequency, the waveguide is cutoff, reflecting the radiation.[17] At frequencies removed from the stop band, the waveguide is transparent and may be used to phase-match nonlinear interactions.[18-19] The region wherein the traveling surface elastic wave perturbs the dielectric waveguide dispersion is indicated in Figure 2. Changes of the surface elastic

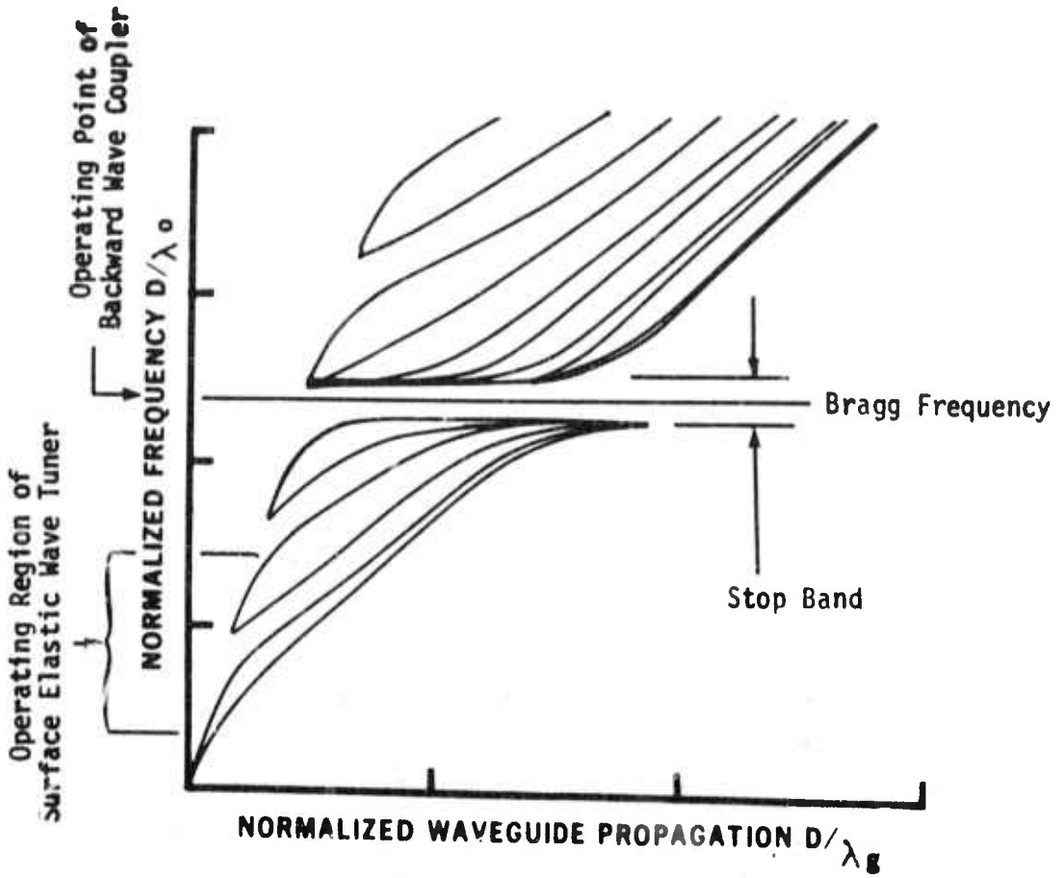

Figure 2. Dispersion of Planar Dielectric Waveguide Containing A Periodic Perturbation.

wavelength and its amplitude will control the dispersion of the feedback waveguide and in turn the integrated CO_2 laser emission wavelength. The frequency shift is the integrated effect of all phase shifts introduced through the entire feedback waveguide. Rapid tuning of the integrated CO_2 laser is limited by the time required for the elastic wave to propagate through the delay line and be replaced by a second different frequency.

B. GAIN AND FREQUENCY CHARACTERISTICS OF THE WAVEGUIDE DISTRIBUTED LASER

The First Interim Technical Report[10] derived in detail a coupled mode theory, giving eigenvalue equations for both the threshold gain and the frequency spectra of a CO_2 waveguide distributed laser having a nonuniform coupling distribution along the laser axis. Approximate solutions of these eigenvalue equations giving the longitudinal mode spectrum and the required threshold gain were also presented. Since these approximations are valid only under low gain conditions, we

present here numerical solutions to the eigenvalue equation valid for a continuous grating structure of length L with a central gap of length ℓ where no coupling exists.[11,12] As will be illustrated in the numerical results, the introduction of the gap into the feedback grating serves to reduce the required threshold gain over the continuous grating case drawing importance in maximizing laser efficiency. In addition, the frequency and gain characteristics of distributed lasers with step-profiles in gain are considered which are important in providing for unidirectional operation in distributed lasers.

1. Nonuniform Coupling in the Periodic Structure

Figure 2a illustrates the configuration for the distributed laser whose operation is based on backward Bragg coupling of waveguide modes by the periodic structure for which propagation constants of the oppositely traveling coupled modes are $|\beta| = \pi/\Lambda$ where Λ is the grating period.

The longitudinal mode spectrum for the distributed laser geometry shown in Figure 3a is determined by solutions of the equation:

$$-\gamma_b \pm i\xi^{\gamma_b \ell} = \gamma_a \coth\gamma_a(L-\ell)/2 \tag{1}$$

where

$$\gamma_b = k_o(n_i - i(1-\frac{\omega_o}{\omega})) \tag{2}$$

$$\gamma_a^2 = \gamma_b^2 + \xi^2 \tag{3}$$

$$\xi \equiv \kappa = \frac{k_o}{\pi} \Delta n_r \tag{4}$$

The parameters $k_o n_i L$ and $k_o L(1 - \omega_o/\omega)$ are taken to be the normalized gain of the active region per pass and the frequency detuning from the Bragg frequency ω_o, respectively. Solutions of (1) simultaneously yield the value of threshold gain necessary for oscillation in the periodic structure and the oscillation frequency.

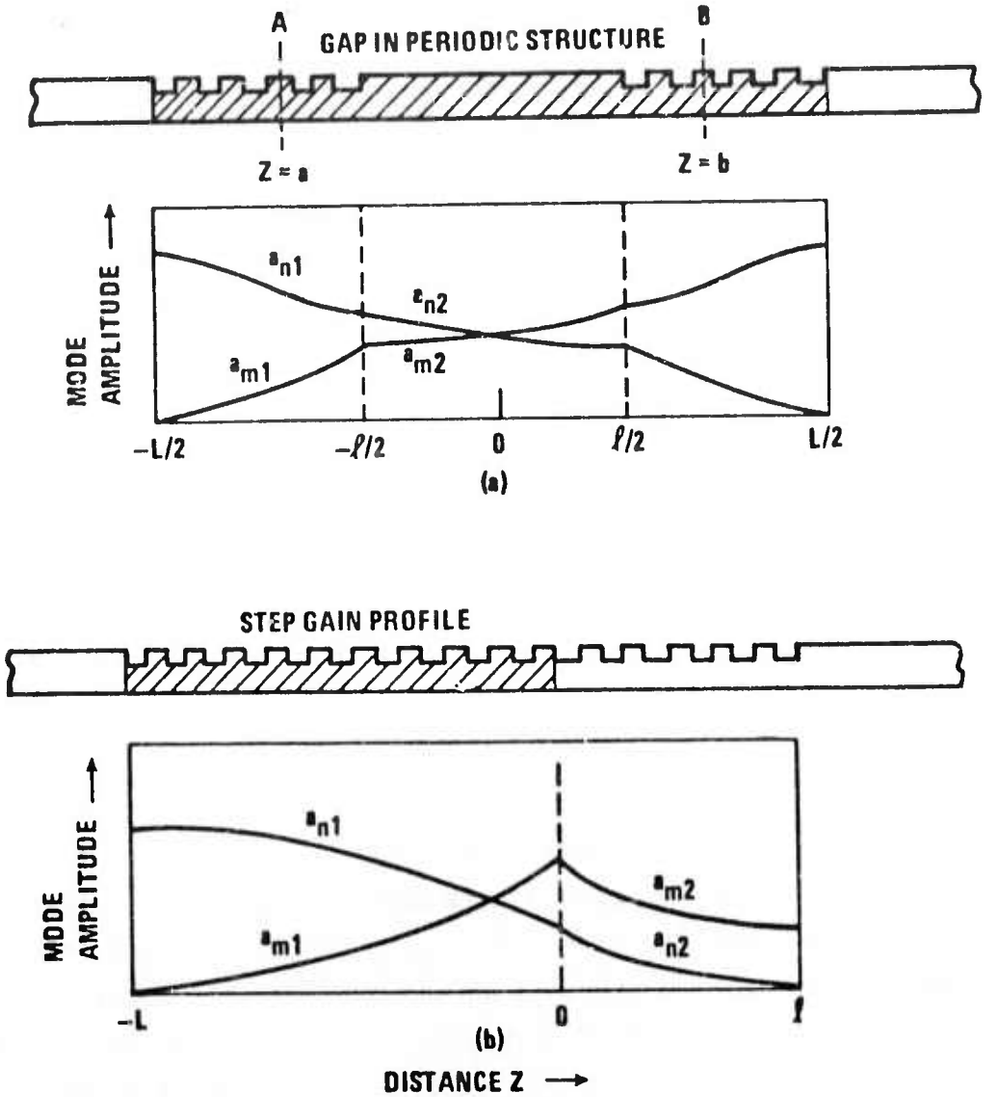

Figure 3. Illustrations of Distributed Laser Geometries and Representative Mode-Amplitude Distributions for (a) Discontinuous Coupling and (b) Step-Gain Profiles.

The mode spectrum is similar to that derived previously for lasers having uniform coupling and gain with some interesting differences. In general, the frequency spectra of distributed lasers consist of longitudinal modes symmetrically located about the Bragg frequency and spaced by frequency increments approximately equal to c/2L. The longitudinal modes, herein designated by the notation L_m where m is an integer denoting the mode order, have different characteristic frequencies

where the higher order modes are located further from the Bragg frequency. As was noted previously (1), no mode occurs at exactly the Bragg frequency when the distributed coupling is provided by a variation in the effective real part of the refractive index of the optical guide.

Figure 4 illustrates the solutions to the eigenvalue equation (1) valid for the geometry shown in Figure 3a. The curves illustrate the parametric behavior of the lasing frequencies $k_0L(1 - \omega_0/\omega)$ and the corresponding threshold gain $(-k_0 n_i L)$ for the first two longitudinal modes L_1 and L_2. The curves are symmetrical about the Bragg frequency so that only half of the spectrum is shown. For a fixed value of the coupling strength κL, the lower order modes have lower threshold gains and a smaller deviation away from the c/2L resonance locations which would exist in a conventional laser of the same length. The frequency "pulling" away from the c/2L points may be observed to be smallest for low values of coupling strength.

A characteristic of the nonuniform geometry which is evident from Figure 4 is that for increased gap lengths ℓ, the mode resonances move closer to the c/2L locations as expected. It may be noted that for large gap lengths, the laser frequency becomes less sensitive to the coupling strength and gain. It is apparent that the threshold gain can be reduced by utilizing the nonuniform geometry, since for constant values of the coupling strength κL the required threshold gain exhibits a minimum. These results suggest that it may be advantageous in the design of distributed lasers to provide a central gap into the periodic structure in order to optimize gain and frequency characteristics. Figure 5 illustrates the variation in threshold gain of the two lowest-order modes for the distributed geometry as the fractional gap length ℓ/L varies. As the gap length approaches unity, the structure closely resembles a conventional Fabry-Perot cavity, and the threshold gain increases without limit because the grating reflectivity approaches zero values. Between this limiting value and that of the continuous grating structure for which $\ell/L = 0$, the threshold gain exhibits an oscillatory behavior, and it is interesting to

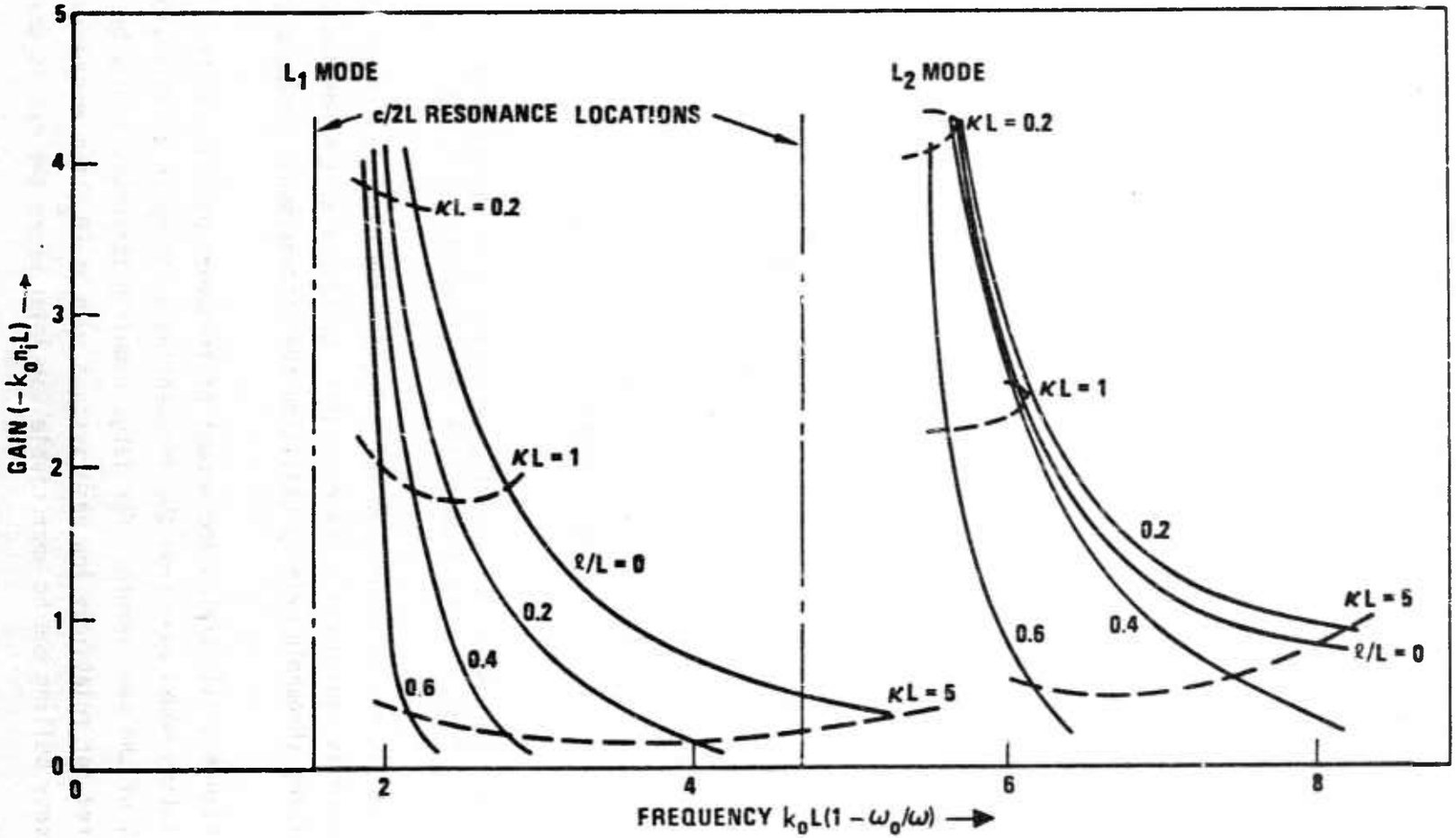

Figure 4. Threshold Gain and Frequency for the Distributed Laser Having a Central Gap of Length ℓ in the Periodic Structure of Total Length L. Two Lowest-Order Modes L_1 and L_2 Are Shown and Dotted Lines Connect Points of Constant Coupling Strength κL.

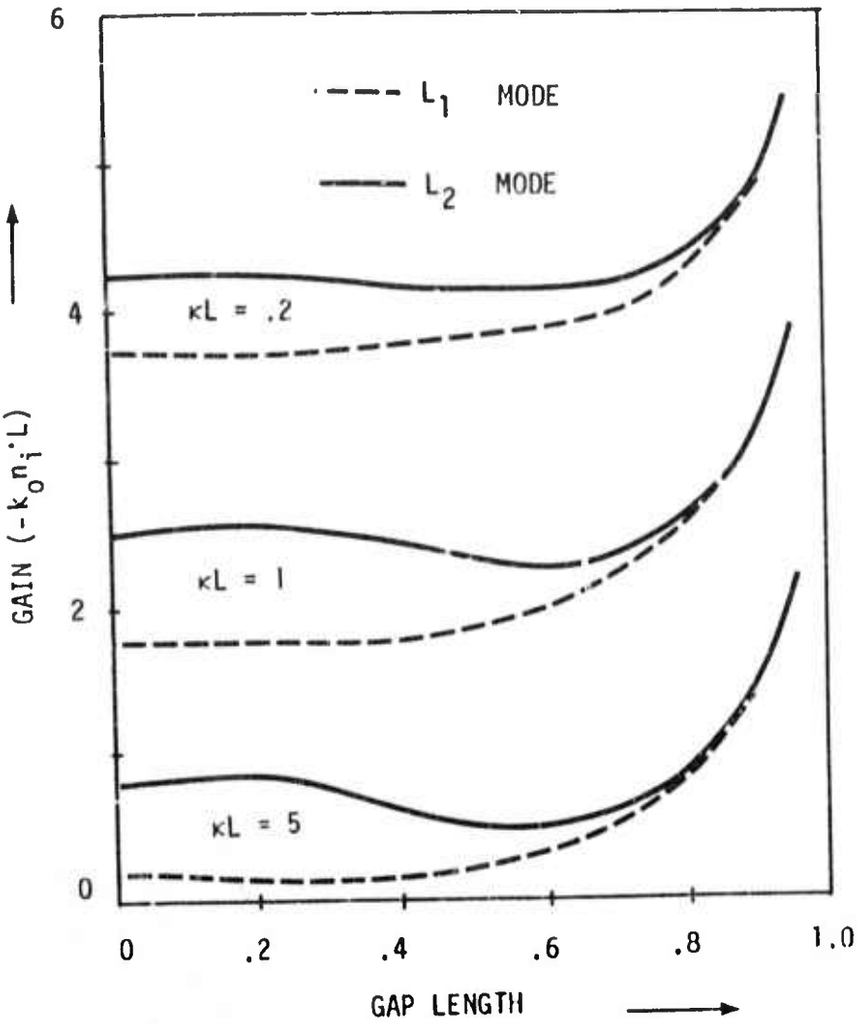

Figure 5. Threshold Gain for the Two Lowest-Order Longitudinal Mode as a Function of the Fractional Gap Length ℓ/L.

note that it may be lower than its value for the case when the grating structure is continuous. These results indicate that the possibility minimizing threshold gain by utilizing the discontinuous feedback structure.

Figure 6 illustrates the amount of frequency pulling of the oscillating modes away from the frequencies existing in a conventional cavity of the same length. For large coupling strengths as may be required for relatively low gain systems such as CO_2, the amount of frequency pulling can be appreciable for laser where the gap is small.

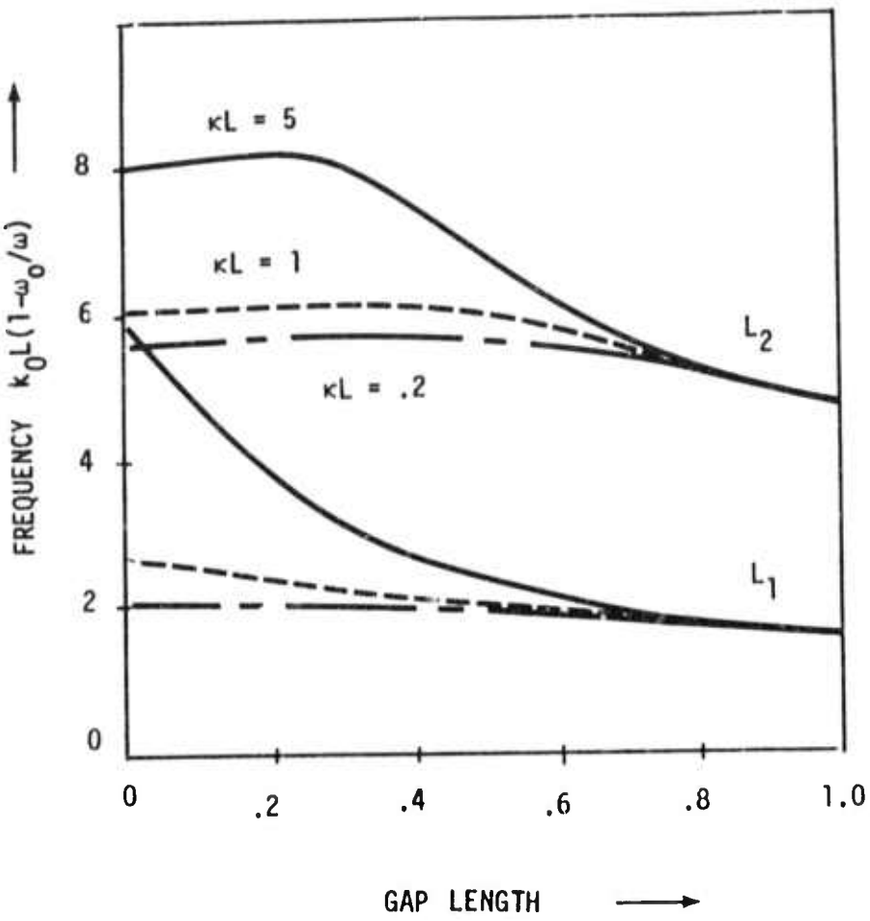

Figure 6. The Oscillation Frequency of the Distributed Laser for the Two Lowest-Order Longitudinal Modes L_1 and L_2 Measured as a Detuning Away From the Bragg Frequency ω_0.

Figure 7 shows the plots of the longitudinal field strength in the laser structure of Figure 3a for several typical values of gap length and coupling. Only the left half of the symmetrical distributions is shown. As may be observed in the diagrams, introducing a central gap into the grating has a pronounced effect on the longitudinal mode distributions at large values of coupling. The dotted curves valid for a continuous grating structure are shown for comparison.

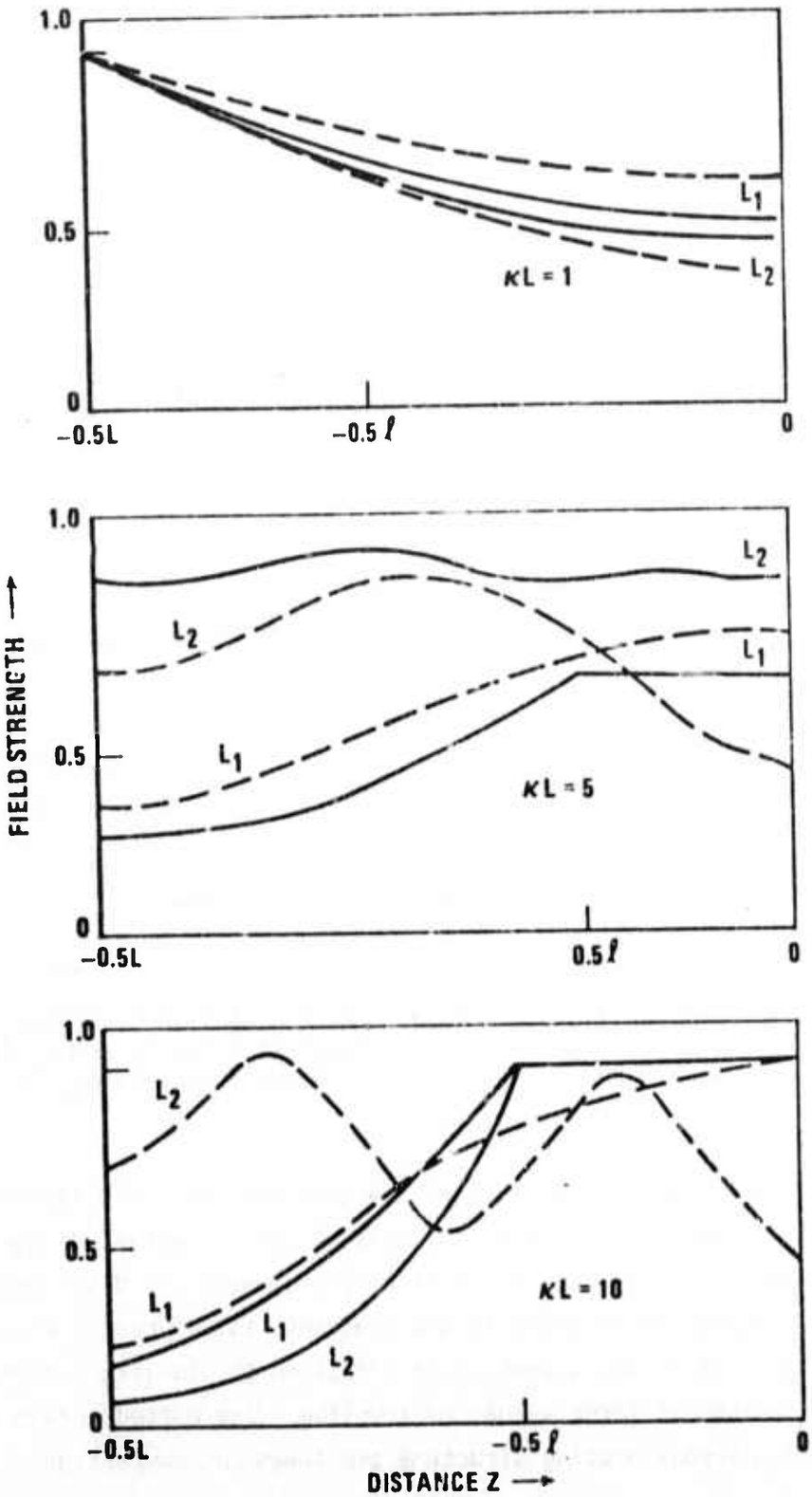

Figure 7. Longitudinal Distributions in the distributed laser for varying gap lengths ℓ/L and coupling. The curves are symmetrical about z=0 and profiles for uniform coupling (ℓ=0) are shown dotted.

2. Step Gain Profile in the Active Medium

Practical future waveguide lasers will require a unidirectional output beam not provided by the symmetrical structures considered heretofore. Asymmetric gain and coupling distributions can result in directionality; however, only a laser geometry having a step function in gain with uniform coupling as illustrated in Figure 3b will be considered here. In the region $z \leq 0$ of Figure 3b having a nonzero gain, the modal solutions take the form:

$$A_{n1} = A_1 \sinh \gamma_1(z + L) \tag{5}$$

$$A_{m1} = \frac{A_1}{i\kappa}\left[\gamma_1 \cosh \gamma_1(z + L) + \gamma_b \sinh \gamma_2(z + L)\right] \tag{6}$$

whereas in the region without gain $z \geq 0$,

$$A_{m2} = A_2 \sinh \gamma_2(z - \ell) \tag{7}$$

$$A_{n2} = \frac{A_2}{i\kappa}\left[-\gamma_2 \cosh \gamma_2(z - \ell) + \gamma_c \sinh \gamma_2(z - \ell)\right]. \tag{8}$$

The eigenfunctions in (5) and (7) result from the imposition of the boundary conditions $A_{n1}(-L) = A_{m2}(\ell) = 0$ again requiring that waves reflected toward the center of the device go to zero at these boundaries. Equations (6) and (8) then follow in a straightforward manner from (60) of the First Interim Report (C72-650.10/501). Boundary conditions imposed at $z = 0$ then result in the eigenvalue equation:

$$\gamma_1 \coth \gamma_1 L + \gamma_b = \kappa^2/(\gamma_2 \coth \gamma_2 \ell + \gamma_c) \tag{9}$$

where γ_b is given by (2) and

$$\gamma_c = -ik_0(1 - \omega_0/\omega). \tag{10}$$

the γ_i's in (9) are given by dispersion relations of the kind

$$\gamma_1^2 = \gamma_b^2 + \kappa^2$$

$$\gamma_2^2 = \gamma_c^2 + \kappa^2.$$

The lasing frequencies and the threshold gains of the laser with a step-profile in gain over a uniform coupling distribution have been computed numerically by solution of (9). Although this lase has asymmetrical longitudinal mode distributions, the mode spectrum is still symmetrical about the Bragg frequency. In effect, the region without gain $0<z<\ell$ acts as a distributed laser "etalon" providing an additional filtering characteristic to the laser output. The threshold gains and frequencies corresponding to the L_1 and L_2 modes of the structure shown in Figure 3b are illustrated in Figures 8 and 9 as a function of this passive etalon length ℓ and may be observed to behave in an oscillatory manner with ℓ. It is interesting to note that for this geometry, the relative threshold gain of the first and second order modes L_1 and L_2 may be controlled by suitably choosing ℓ/L. At a value of $\ell/L \approx .5$ for example, the threshold gain for the L_1 mode may be reduced while simultaneously increasing the gain threshold for the second order mode. This effect becomes useful in distributed laser devices where improved higher order mode rejection is required. Calculations directly from the curves of Figure 8 show that the higher-order-mode rejection can be improved by about 4db for structures with $\kappa L \approx 1$ and as much as 7db for high gain lasers with lower coupling strengths.

It is worthwhile to note that for low values of coupling in the step-gain geometry, it is possible for the second order mode L_2 to have a lower gain threshold than the L_1 mode as evidenced by the crossover of the gain curves in Figure 8. Although not apparent in Figure 8, the oscillatory behavior of the curves damps out to a constant final value when the length of the passive structure becomes very long, as expected. Under these conditions, the laser becomes almost unidirectional since one end of the laser then sees a highly reflective structure.

Figure 8 illustrates the longitudinal mode distributions of the distributed laser shown in Figure 3b for the two etalon lengths ℓ denoted by dotted lines in Figure 10a. At $\ell = .5L$, the resulting field-strength distributions for the L_1 and L_2 modes are substantially dif-

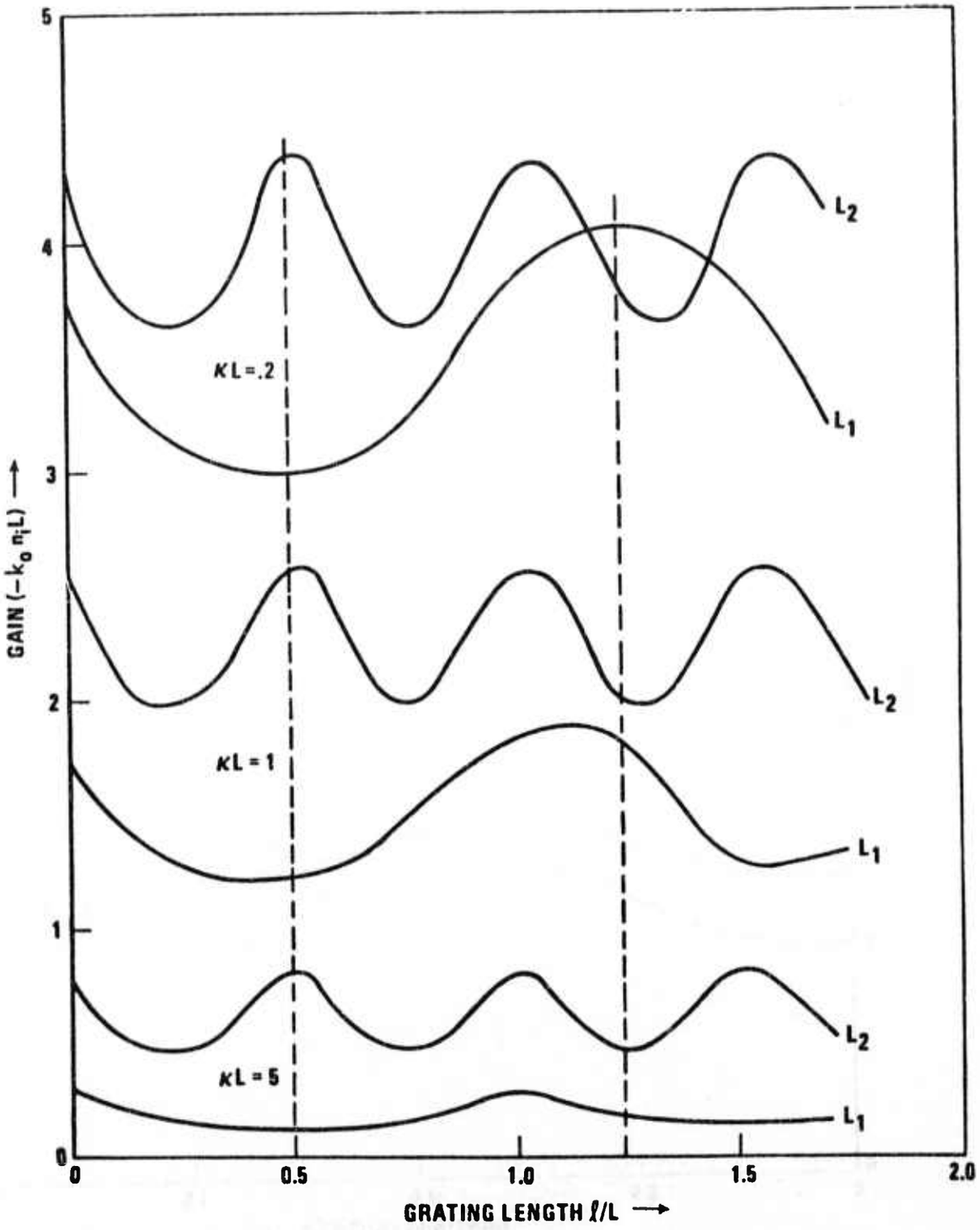

Figure 8. Threshold gain required for the distributed laser with a step-profile in gain where L and ℓ are the lengths of the active and passive regions, respectively. The two lowest-order modes L_1 and L_2 are shown.

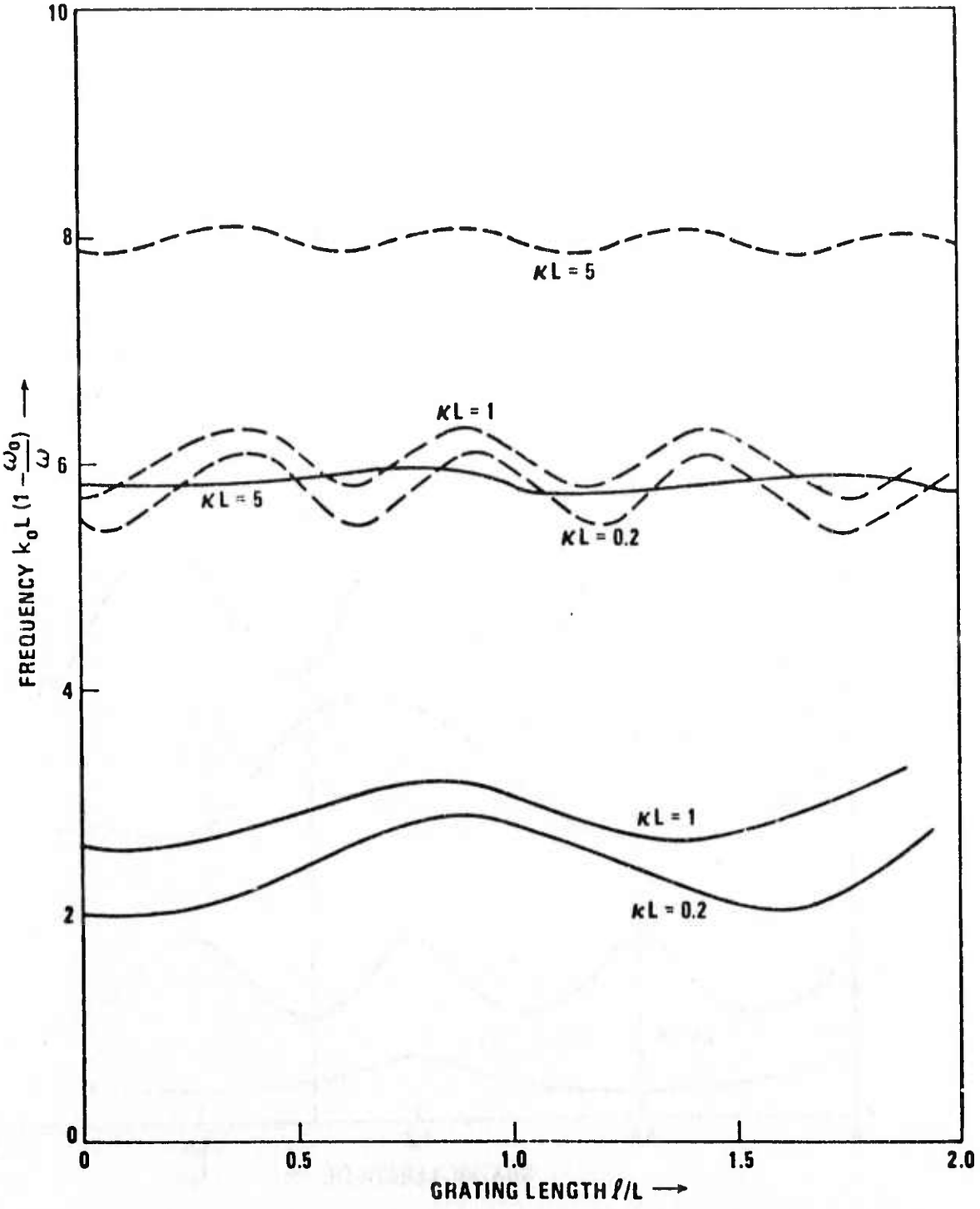

Figure 9. Oscillation frequency at threshold corresponding to the gain solutions of Figure 8.

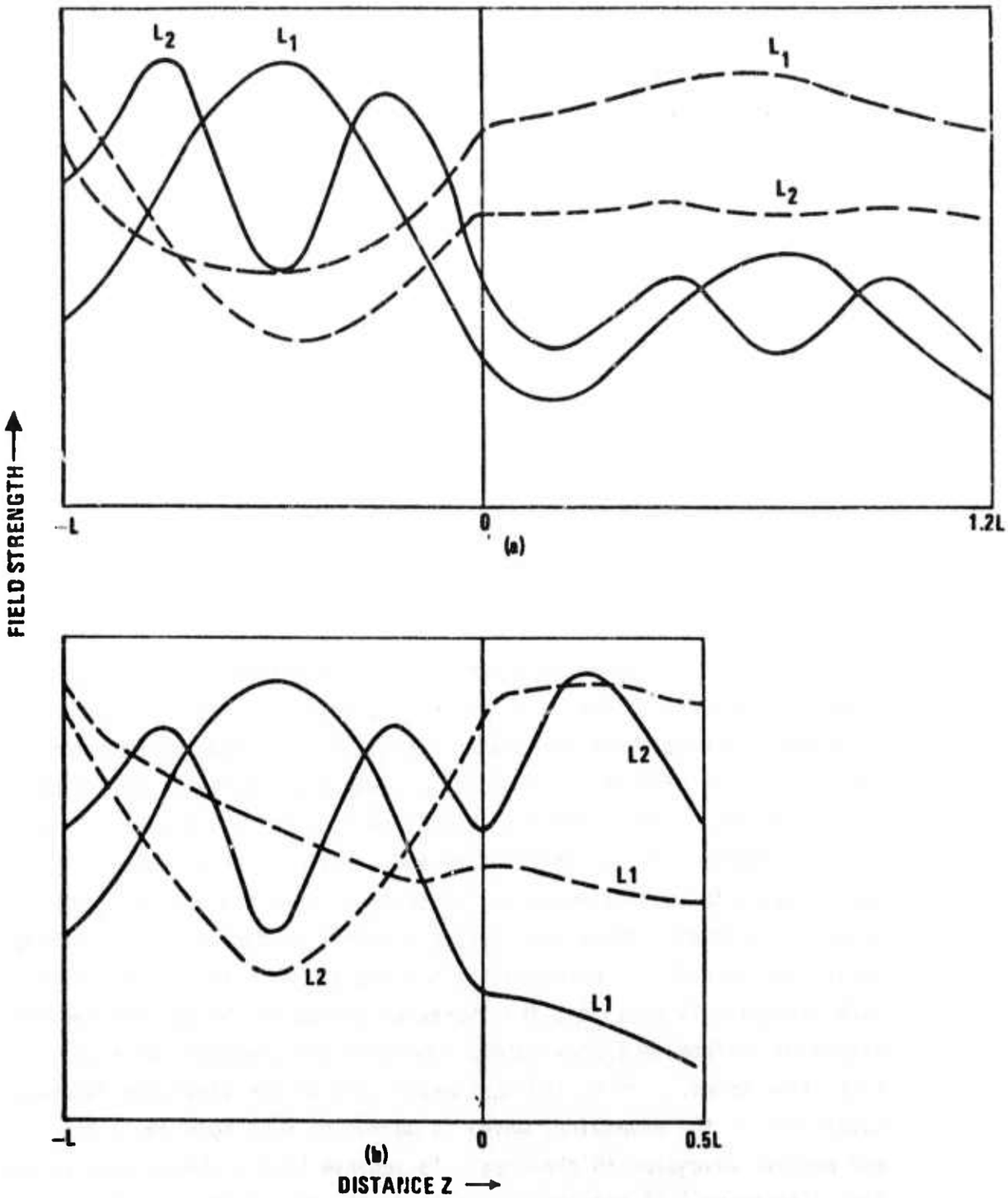

Figure 10. Longitudinal distributions of electric field strength in the distributed laser with a step-gain profile for two ratios of passive to active-waveguide lengths shown dotted in Figure 8, (a) $\ell/L = 1.2$, (b) $\ell/L = 5$. Dotted lines are for $\kappa L = 1$ and solid lines $\kappa L = 5$.

ferent corresponding to the large difference in threshold gain. However, for $\ell = 1.2L$, which results in smaller difference in threshold gains between the L_1 and L_2 modes the mode patterns have greater similarity. The general character of the mode patterns is similar to that observed previously for lasers with uniform coupling and gain except that there exists an asymmetry in the field strength at the two ends of the structure resulting in directional output characteristics. For example, we may compute from Figure 10a that the L_1 mode for the structure having $\kappa L = 5$ should have a directional output with a forward-to-backward ratio of about 12db.

C. DISTRIBUTED FEEDBACK GRATING PROCESSING

The experimental effort devoted to the production of the passive feedback waveguide and the backward wave Bragg diffraction couplers are delineated in this section.

The photolithographic requirements to produce the backward wave Bragg diffraction couplers are much more severe than those employed to produce an electronic integrated circuit.[20] The grating must extend over dimensions of 3 mm width and 10 cm length preserving parallelism and uniformity of the grating perturbation to a small fraction of the CO_2 wavelength. The grating grooves and walls must have optically smooth edges to prevent Rayleigh scattering. When the active waveguide is employed without the passive feedback waveguide, the iterative period in the wall is approximately 5 microns. When the passive feedback waveguide is employed, the iterative period in the passive feedback waveguide surface is approximately 3 microns and dependent upon its refractive index. The period must match that of the vibration-rotation wavelength in the waveguide, which is dependent upon both the active and passive waveguide thicknesses. To achieve high backward wave reflection efficiency[21,22] requires a groove depth comparable to $\lambda_0/2$ which is an extraordinary depth requirement of the photolithographic process.

Definition of the grating groove walls by chemical etches produces a comparatively rough surface due to a variety of defects.[20] Chemical

etches also undercut the pattern definition mask, the amount of which depends upon the agitation. The use of RF reverse sputtering (ion etching) provides a superior definition of the perpendicular walls accurately conforming to the mask without undercutting. The use of this procedure requires a mask relatively immune to ion bombardment in comparison to the substrate. A process technique to achieve the required grating surface topology has been successfully developed for this program.

A delineation of this photographic planar processing technique follows. The gratings are produced by interference of coherent ultraviolet radiation both in photographic emulsions subsequently transferred to photoresist and directly in the photoresist. The procedure is not described further herein because it conforms to standard practices.[23,24]

The processing sequence to produce deep groove gratings is illustrated in Figure 11. The procedure is essentially that of production of a mask in a metallic film by photography and chemical etch, such that the metallic film can serve as a subsequent mask during the ion etching. Various metallic films have been investigated such as Au, Al, Ta, and Ti, most of which have been oxidized to improve their resistance. The use of titanium is preferred. During this investigation, pyrex glass substrates were employed because they are relatively impervious to ion etching, particularly with a polished work-hardened surface, and because it is amorphous.

Referring to Figure 11, a specific processing procedure is outlined as an example.

1. (Section A) The deposition of a thin titanium film (~8000 Å) on an optically polished substrate of pyrex glass with dimensions of 2 x 10 cm is followed by the application of a photoresist film (AZ111) diluted (1:1) solution, by spinning of the substrate at ~ 5000 Rpm for 16 seconds. The resulting photoresist film has a uniform thickness of 1μm, and it is dried at 90°C for 30 minutes.

2. (Section B) Direct projection of the desired image is performed or contact printing of the grating pattern is performed using a large area collimated uv source.

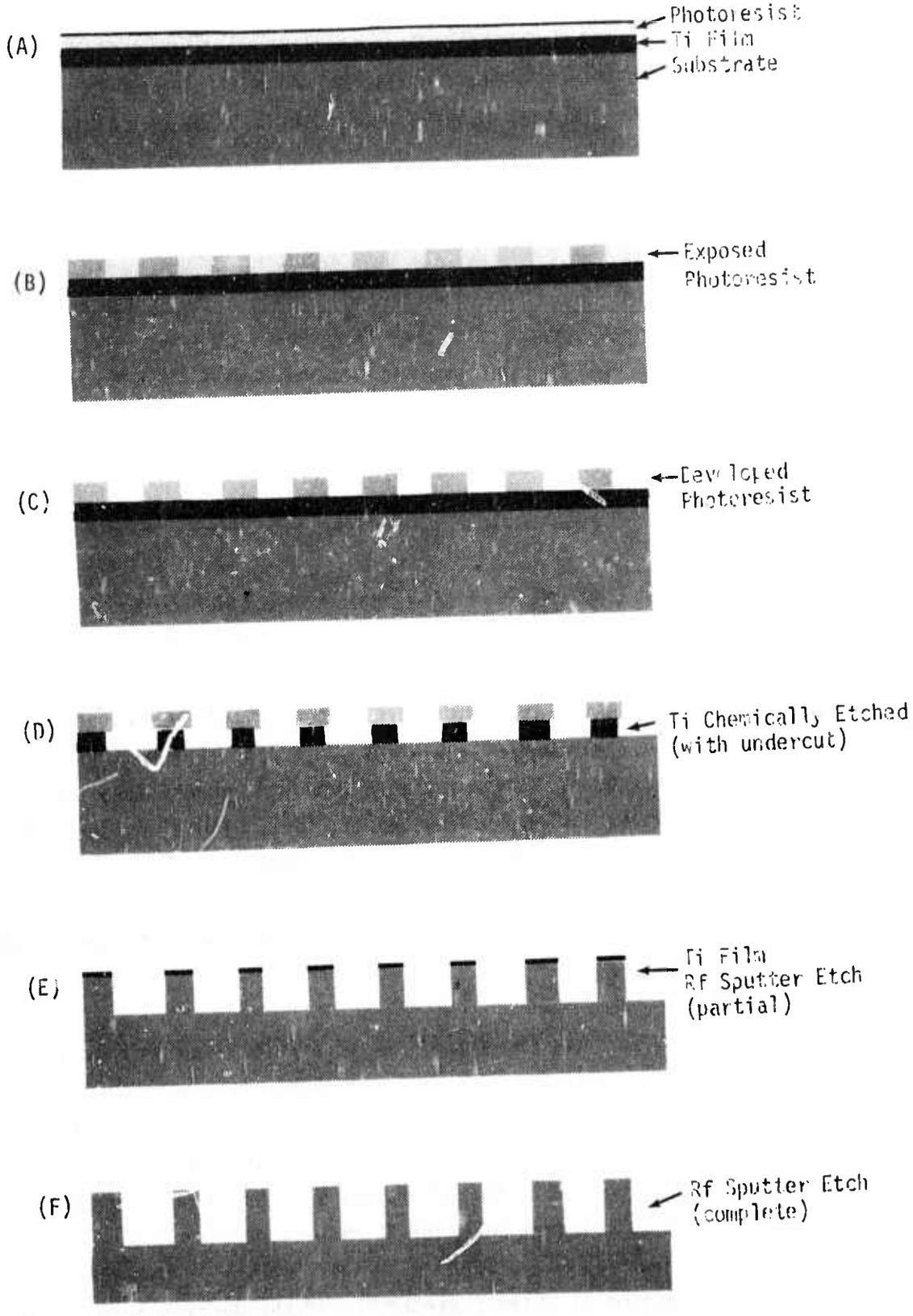

Figure 11. Processing Sequence for Deep Patterns (Diffraction Grating)

3. (Section C) After development of a photoresist and additional heat treatment at 95°C, the exposed Ti film is etched in a solution of 20 parts H_2O: 1 part HF: 1 part H_2O_2, which is compatible with the AZ111 photoresist. The etching rate of evaporated Ti in this solution is on the order of 150 Å/second. In some cases, the etching time is extended to allow a slight "undercutting" of the photoresist to insure that the residual Ti is completely removed.

4. (Section D, also see Figure 12) Prior to the insertion in the sputtering chamber, the substrates are thoroughly cleaned in deionized H_2O, maintaining the residual photoresist pattern on the Ti to enhance the masking.

5. RF reverse sputtering (ion etching) -- the sputtering system (MRC5") is evacuated to 10^{-6} torr and backfilled with a mixture of 10% O_2 and 90% Ar, resulting in a final background pressure of 10^{-4} torr. For a 10 cm grating pattern, the optimum reverse sputtering parameters were established at a cathode distance of 7 cm with 400 W RF power applied. The removal rate of Ti in this configuration is ~40 Å per minute, while the removal rate of pyrex is 120 Å per minute (Section E). The reverse sputtering process is continued until the Ti film is completely removed (Section F).

The quality of the pattern definition, in this case a grating, is determined by either a Tolansky, Mirau, or Michelson interference microscope photograph, or by the use of a stylus profile, or by measurement of the grating diffraction efficiency.[25,26] A transmission photomicrograph is illustrated in Figure 12. After completion of Step 4, the mask is an exact replica of the photographic emulsion produced by interference of coherent uv beams. The comparatively narrow lines are achieved by overexposure, utilizing only the null of the fringe pattern. Irregularities of the lines are due to imperfections of the interferometer rather than due to any step of the processing.[10] Figure 13 illustrates a stylus profile of transmission grating produced in a pyrex substrate using a Ti mask. The groove depth of this particular example is 1.5 microns. The true profile of the grating is obscured by the convolution of the stylus.

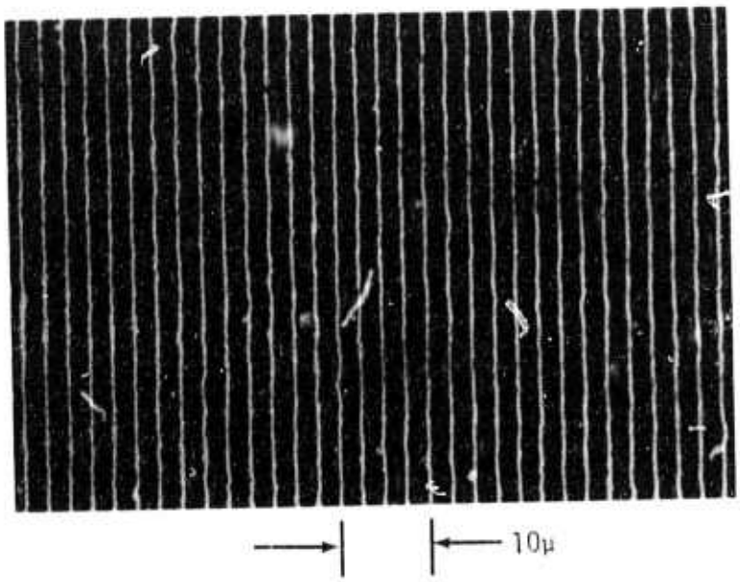

Figure 12. Transmission photograph through developed photoresist, chemically etched Ti, and pyrex substrate (master in photograph emulsion).

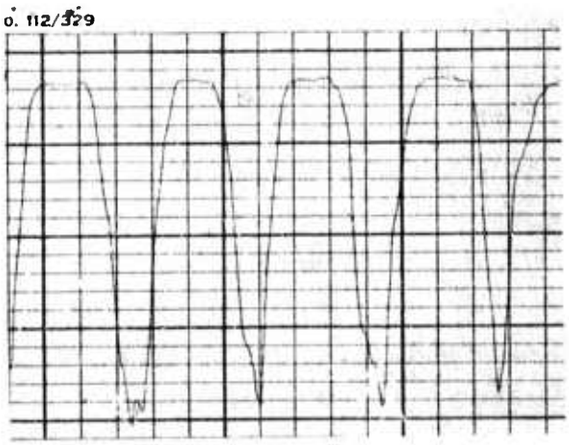

Figure 13. Stylus profile of diffraction grating--thickness 1.5 microns--achieved through use of a Ti mask.

The deep groove photolithographic process has been established for substrates such as pyrex which is relatively immune to ion bombardment. It is, therefore, applicable to all materials responsive to RF reverse sputtering such as required to form the passive feedback waveguide with its distributed feedback grating. In the expecta-

tion that a collinear surface elastic wave would be employed to tune the passive feedback waveguide dispersion, experiments have been concentrated upon the use of Te and As_2Se_3 as suitable materials for the passive feedback waveguide because they exhibit the largest and next largest known elasto-optic figure of merit, respectively. A deposition technique based upon evaporation has been employed successfully. Successful depositions have been deposited upon NaF, BaF_2, NaCl and ZnS single crystals, and on polycrystalline ZnS as well as glass. The results using Te show excessive absorption and a low damage threshold in the 10 μ region. Films of As_2Se_3 exhibit a low absorption; namely, 0.005 cm^{-1}. Therefore, As_2Se_3 will be employed as the passive feedback waveguide including a distributed feedback grating and an output grating.

To launch the surface elastic wave on the substrate collinear with the passive feedback waveguide requires either a bulk piezoelectric wave transducer and mode converter or a piezoelectric thin film with interdigital transducer. Deposition techniques to produce piezoelectric thin films of ZnO and CdS are well established. These films are piezoelectric because of ordering in one axis aluminum nitride thin films are also piezoelectric exhibiting a large coupling coefficient. To investigate the absorption of AlN at 10 μ, a thin film was deposited upon Si epitaxially followed by removal of the Si and measurement of its transmission. A suitable, comparatively narrow transmission window was observed in the 10 μ micron region.

The use of the electro-optic effect is an alternative to the elasto-optic effect. The preferred electro-optic materials are CdTe and GaAs because of their large coefficients and low absorption. They require excessive drive power to affect the required tuning unless employed in a waveguide configuration. Unambiguous tuning combining an electro-optic Fabry-Perot and a distributed feedback ring resonant circuit may be achieved as coupled resonant circuits.[16]

D. PLANAR WAVEGUIDE CO_2 LASER PLASMA DISCHARGE

The initial effort[10] identified the production of a continuous uniform transverse plasma discharge constrained by the waveguide walls as a serious problem. Both DC and RF excitation yielded concentrated arcs in the thin waveguide section. The thin plasma discharge waveguide chamber differs drastically from that of the large chambers employed for transverse excited atmospheric CO_2 laser designs which operate only in the pulse mode.[9,27]

A major portion of this reporting period has been directed toward the general fundamental problem of experimentally producing a continuous uniform plasma discharge largely via Rockwell International funds. Various facets of this investigation are delineated herein.

A hollow planar waveguide CO_2 laser was successfully demonstrated using a waveguide height of 500 μ. The experiment employed a transverse array of pin cathodes (31) resembling a comb. The anode was a continuous copper strip with the edge exposed to the transverse discharge constriction. The total gas pressure employed was 80 Torr of CO_2: N_2: He at proportions of 1:1:2. Thus, a DC transverse excitation and transverse flow were employed.

The Fabry-Perot employed miniature planar reflectors within the waveguide rather than the intended distributed feedback grating structure. The planar reflectors were fabricated from small chips of GaAs inserted as the vacuum wall with an Al film to produce 100% reflectivity. The output was taken by scratching the center section to create in effect a slot coupler approximately 5 μ wide. The resulting beam appears as a fan with an approximate output of 10 mW. Optimization of the gas pressure composition was not adequately performed. A polycrystalline BeO gas manifold as the waveguide superstrate together with a pyrex waveguide substrate contained the plasma discharge. The BeO superstrate external surface was maintained at -30°C. The effort to reproduce the experiment in 100 μ high waveguide was unsuccessful presumably due to contamination of the Fabry-Perot faces by vacuum grease.

To support the feasibility of designing waveguide lasers with reduced cross section, a hollow capillary laser with a bore diameter of 600 μ was successfully demonstrated. Longitudinal flow and discharge at -70°C was employed. The operation was degraded by the high capillary gas flow impedance. The capillary was formed from fused silica with a wall thickness of 1 mm. The above rectangular cross section and circular cross section waveguide lasers represent the smallest thus far demonstrated for CO_2. The experiments confirm the increased gain due to the close proximity of the waveguide walls.[3,9,13]

A plan view of the comb cathode, strip anode plasma discharge across the waveguide constriction (full size) is illustrated in Figure 14. Parameters of the discharge illustrated in Figure 14 include total pressure 160 Torr, 1:1:2, waveguide height of 250 μ; 10 KV, 4.00 mA across and through 31 ballast resistors 7.2 M Ω. Although laser operation was obtained using the discharge illustrated in Figure 14, the uniformity, stability, and life are not considered adequate.

The transverse cross section of the plasma discharge chamber used for this investigation is illustrated in Figure 15. Several electrode configurations investigated are illustrated in the figure. They include: (1) a vertical strip anode and pin cathode array, (2) a vertical strip cathode and anode on each side of the waveguide constriction, and (3) a strip cathode and anode on the bottom of the gas manifold, adjacent to the waveguide constriction. The electrode strips on the bottom have been tapered to improve the discharge uniformity. Figure 16 illustrates the discharge from the latter configuration using a strip cathode and anode at the bottom of the channel. The waveguide thickness is 175 μ. Although the discharge of Figure 16 appears more uniform than that of Figure 14, it is in fact not. The exposure time of Figure 16 is 1/2 second, while that of Figure 17 under identical conditions is 1/500 second. The total pressure of Figures 16 and 17 is 160 Torr in proportions of 1:1:2. The discharge will be initiated at approximately 10 Kv to extend the discharge over the entire 9 cm length.

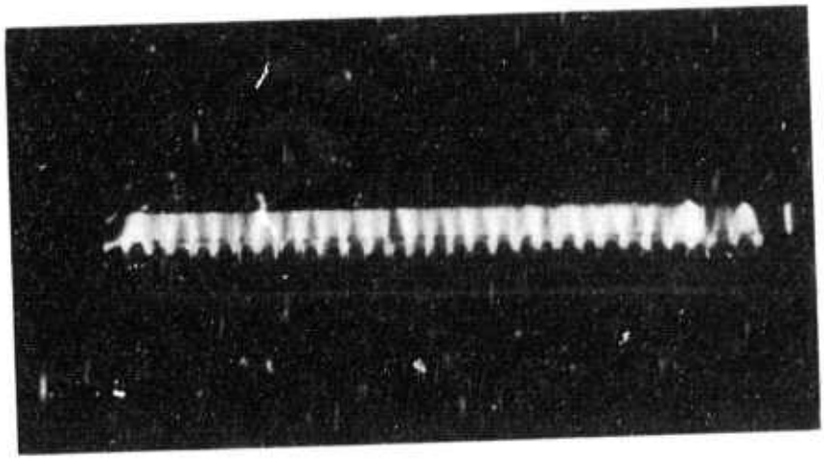

Figure 14. Plan view of CO_2 discharge used for planar waveguide laser - 9cm long, 5mm wide, pressure 160 Torr using comb cathode/strip anode with external ballast resistors

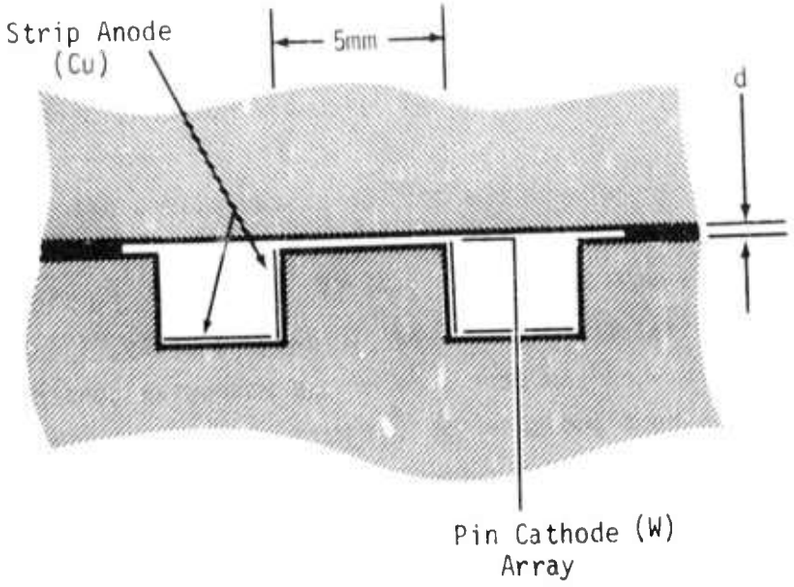

Figure 15. Transverse cross-section of planar waveguide and CO_2 plasma discharge chamber

Some typical results of the investigation to produce a continuous transverse CO_2: N_2: He discharge are illustrated in the photographic collage--Figures 18, 19, and 20. The active waveguide height in each case is 1 mm. The top of each figure corresponds to the anode while the bottom corresponds to the cathode. Both cathode and anode are formed by thick conductors in the bottom of the gas manifold (see

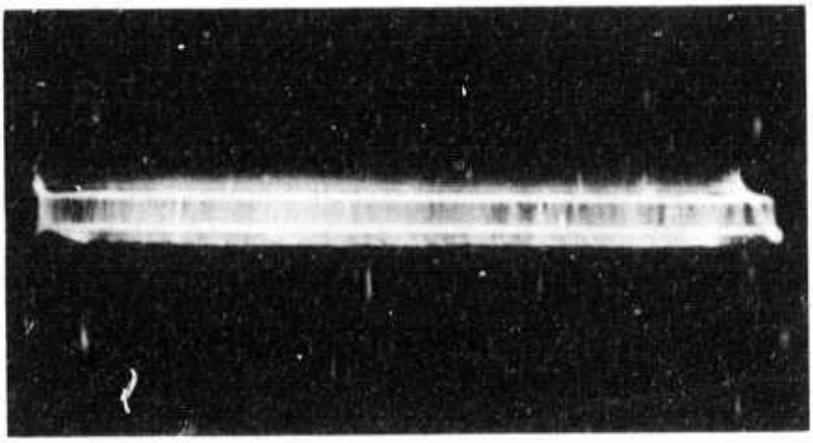

Figure 16. Plan view of CO_2:H_2:He plasma discharge using strip cathode and anode at bottom of channels - waveguide thickness 175 μ, photographic exposure 1/2 sec (full scale)

Figure 17. Same as Figure 16. Photographic exposure 1/500 sec (1/2 scale)

Figure 15). However, they have been shaped to approximate the Rogowski profile.[27] Figure 18 illustrates that end effects have been eliminated in the discharge by control of the electrode design. The true glow discharge of Figure 18 at 1 Torr employs air. Using an appropriate CO_2 mixture, the pressure has been increased to 6 Torr in Figure 19, which shows the appearance of a dark space around and over the waveguide constriction. Increasing the pressure to 300 Torr and increasing the He composition, the effect upon the discharge is illustrated in Figure 20. The scale of Figures 18, 19, and 20 is identical. Movement of the discharge in Figure 20 to the left arises because of the pressure differential along the gas manifold. The discharge in Figure 20 appears at the low pressure end. The total transverse current in

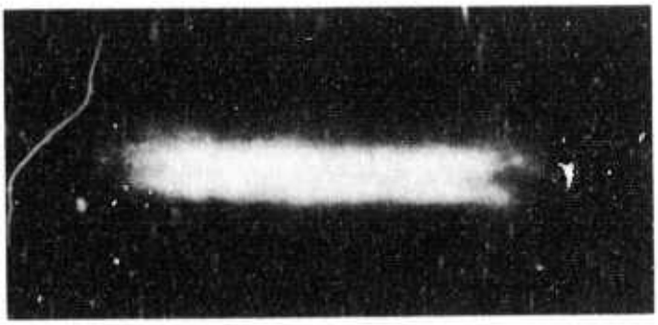

Figure 18. Continuous transverse DC excitation, pressure 1 Torr $N_2:O_2$ 5:1, d = 1mm (strip cathode and anode)

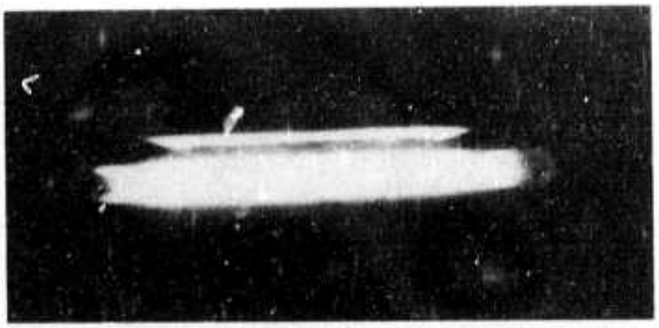

Figure 19. Same as Figure 18 except pressure 6 Torr $CO_2:N_2$:He 1:1:2 — cathode dark space appears in waveguide section (~ Rogowski cathode and anode profile)

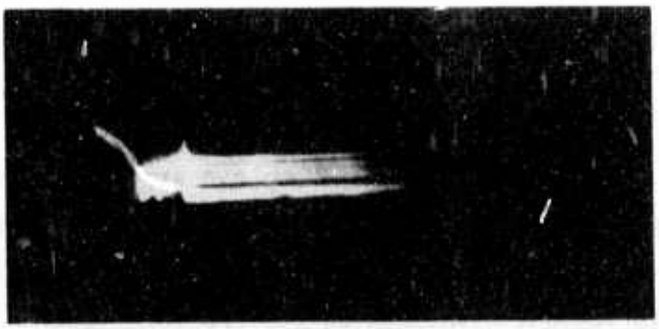

Figure 20. Same as Figures 18 and 19 except pressure 300 Torr $CO_2:N_2$:He 1:1:4 — glow occurs in waveguide section non-uniformity due to pressure gradient

Figure 18 is 0.6 mA, 13 mA in Figure 19, and 8 mA in Figure 20, which corresponds to the optimum ballast resistance for each case. At the highest pressure in Figure 20, the discharge is oscillatory, indicating some glow to arc transition, and thus the stability is unacceptable.

The discharge illustrated in Figure 19 is representative of the mid-pressure range. The position of the dark space is pressure and current dependent. The long continuous glow illustrated in Figure 19 (7 cm) breaks up into multiple glow segments as the current is reduced by an increase of the ballast resistance. When the total discharge current is reduced by an order of magnitude, a single concentrated glow occurs approximately 5 mm wide. When conditions are set up which lead to reduced glow width in the waveguide section, the corresponding glow over the cathode region remains several times larger.

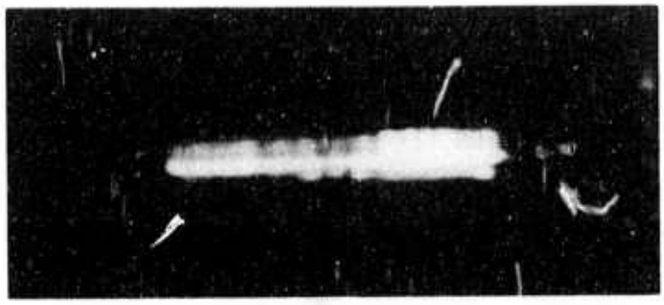

Figure 21. Same as Figure 20 except transverse pulsed excitation

The plasma discharge structure, pressure, and composition illustrated in Figure 20 has been employed using a transverse pulsed excitation with a result illustrated in Figure 21. The pulse was 1.5 KV with microseconds width, with a repetition period of 2 milliseconds. Note that the concentrated glow has shifted to the high pressure end and is more diffuse.

Several conclusions can be drawn from our investigation of continuous transverse excitations across constricted chambers. In order to obtain a uniform wide-area transverse discharge, independent means must be used to control electron temperature and number density. Further exploration of transverse excitation will employ a combination of pulsed excitation with a DC sustaining electric field.

As an alternative to the investigation of the transverse excitation, consideration has also been given to a longitudinal approach providing for either a longitudinal or transverse flow. The results of an experiment showing a continuous longitudinal discharge in a planar waveguide structure is illustrated in Figure 22. The waveguide height is 1 mm. The waveguide width is 3 cm.

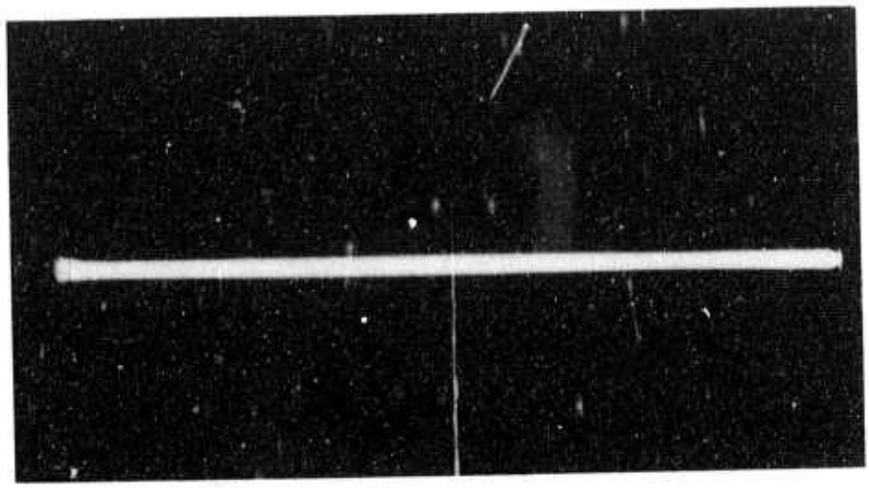

Figure 22. Continuous longitudinal CO_2:N_2: He discharge in planar structure, pressure 10-300 Torr 1:1:2, d=1mm longitudinal flow - discharge 15cm long, ~4mm wide

The discharge width is approximately 4 mm. The discharge location in the wide waveguide is stable using a longitudinal flow throughout the 3 cm width. The discharge width is pressure dependent, being larger at low pressure. The discharge observed is stable and uniform throughout the pressure range of 10 to 300 Torr. Experiments have been performed with CO_2: N_2: He in proportions of 1:1:2. Substantial increases of the He proportion do not alter the discharge characteristics. It is interesting to note that this discharge characteristic width is the same as that observed in the transverse conditions with reduced current. The planar longitudinal discharge sustaining voltage is approximately 1/2 that of a circular capillary with the same transverse dimensions.

The ease and simplicity of creating and the resultant uniformity and stability of the longitudinal discharge merits serious consideration as an alternative to the transverse approach. The problem of introducing the discharge through the waveguide walls can be circumvented by extending the discharge further than the distributed feedback structure's length.

III. REVIEW

A. CONCLUSIONS AND RECOMMENDATIONS

Emphasis during this reporting period has largely been devoted to an investigation of experimental techniques to produce a continuous uniform transverse plasma discharge. The results have been marginally successful with the demonstration of laser operation using a pin comb cathode array at 80 Torr. The required potential to sustain the transverse discharge is much less than that required for a comparable capillary.

An investigation of concepts to produce a continuous uniform transverse discharge continues to be encouraging and justifies optimism. However, the ease of producing a longitudinal discharge confined by planar super- and substrate waveguide walls with uniformity ans stability has stimulated its future consideration on an equal par with that of the transverse excited planar structure. The required electric field to sustain a longitudinal excitation in a planar structure is approximately 1/2 that required in a circular capillary.

Our understanding of the continuous transverse planar plasma discharge excitation now seems to be on firm ground. A true glow discharge can be created over a wide pressure range. The transverse dimensions generally become severely restricted (approximately 4 mm) as the pressure is increased to 300 Torr. Attempts to increase the transverse dimension seems to lead to spatial instabilities. The electron recombination becomes dominant as the wall spacing is reduced below 1 mm and when coupled with thermal effects readily leads to avalanche processes. Some of the instabilities observed are due to end effects of the electrodes while others arise from the slight transverse pressure gradient.

It is now clearly evident that an excess of electrons must be supplied to the discharge in the waveguide region similarly as currently employed in the larger transverse excited atmospheric CO_2 lasers. One means to be investigated herein will employ a pulse excitation to generate the required electron density and a sustaining continuous field to control the electron temperature.[27]

B. PLANS

The effort thus far has demonstrated a circular capillary waveguide laser with bore diameter of 600 μ using longitudinal excitation and flow and a planar waveguide CO_2 laser with a waveguide height of 500 μ using transverse excitation and transverse flow. These are, apparently, the smallest waveguide dimensions thus far demonstrated at CO_2 wavelengths. Although the effort will continue to explore the transverse excitation and transverse flow, the effort will now also include longitudinal excitation in a planar structure using either longitudinal or transverse flow without the waveguide width constriction.

The photolithographic processing art to achieve long uniform deep groove diffraction gratings has now been sufficiently developed for application in the planar CO_2 waveguide structure. The optimum material for use as the passive waveguide in combination as the distributed feedback is believed to be As_2Se_3. Replacement of the miniaturized Fabry-Perot reflectors with the backward wave Bragg diffraction couplers, measurement of gain losses as a function of the waveguide height is the next immediate step determining the selection of the interaction effect to achieve tuning.

C. ACKNOWLEDGEMENTS

Deposition of Te and As_2Se_3 thin films on a variety of substrates by Dr. M. F. Ehman is sincerely appreciated.

D. REFERENCES

1. E. A. Marcatile and R. A. Schmeltzer, "Hollow Metallic and Dielectric Waveguides for Long Distance Optical Transmission and Lasers," BSTJ 43, 1783 (1964).

2. P. W. Smith, "A Waveguide Gas Laser," Apply. Phys. Letters 19, 132 (1971).

3. T. J. Bridges, E. G. Burkhardt and P. W. Smith, "CO_2 Waveguide Lasers," Appl. Phys. Lett. 20, 403 (1972).

4. E. G. Burkhardt, T. J. Bridges and P. W. Smith,"BeO Capillary CO_2 Waveguide Laser," Optic Comm. 6, 193 (1972).

5. R. E. Jensen and M. S. Tobin, "CO_2 Waveguide Gas Laser," Appl. Phys. Lett. 20, 508 (1972).

6. J. J. Degnan, H. E. Walker, J. H. McElroy, N. McAvoy and T. Zagwodski, "A Curve-Fitting Technique for the Determination of Gain and Saturation Intensity in Homogeneously-Broadened Gas Lasers: Application to a Waveguide CO_2 Laser," Goddard Space Flight Center, Report X-524-72-38) Oct. 1972.

7. R. L. Abrams and W. B. Bridges, "Characteristics of Sealed-Off Waveguide CO_2 Lasers, 1973 IEEE/OSA Conference on Laser Engineering and Applications, Washington, D. C.

8. R. Yusek and G. Lockhart, "CO_2 Waveguide Laser," 1973 IEEE/OSA Conference on Laser Engineering and Applications, Washington, D. C.

9. P. W. Smith, P. J. Mahoney, and D. R. Wood, II, "A Waveguide TEA Laser," 1973 IEEE/OSA Conference on Laser Engineering and Applications, Washington D. C.

10. D. B. Anderson and R. Shubert, "Tunable 10 Micron Laser, An Integrated Approach to Infrared Gas Laser," Interim Technical Report C72-650.10/501, Rockwell International, February 26, 1973.

11. R. Shubert and D. B. Anderson, "Characteristics of Nonuniform Distributed Feedback Waveguide Lasers," 1973 IEEE/OSA Conference on Laser Engineering and Applications, Washington, D. C.

12. R. Shubert, "Theory of Optical Waveguide Distributed Laser with Nonuniform Gain and Coupling," to be published.

13. P. W. Smith and P. J. Mahoney, "A Self-Stabilized 3.5 μm Waveguide He/Xe Laser," Appl. Phys. Lett. 22, 667 (1973).

14. D. Marcuse, "Hollow Dielectric Waveguide for Distributed Feedback Lasers," IEEE, JQE 8, 661 (1972).

15. H. Kogelnik, C. V. Shank and J. E. Bjorkholm, "Hybrid Scattering in Periodic Waveguides," Appl. Phys. Lett. 22, 135, (1973).

16. P. W. Smith, "Mode Selection in Lasers," Proc. IEEE 60, 422 (1972).

17. F. W. Dabby, M. A. Saifi and A. Kestenbaum, "High-Frequency Cut-off Periodic Dielectric Waveguides," Appl. Phys. Lett. 22, 190 (1973).

18. S. Somelb and A. Yariv, "Phase-Matchable Nonlinear Optical Interactions in Periodic Thin Films," Appl. Phys. Lett., 21, 140 (1972).

19. F. W. Dabby, A. Kestenbaum and U. C. Paek, "Periodic Dielectric Waveguides," Optic Comm. 6, 125 (1972).

20. D. B. Anderson and R. R. August, "Application of Microphotolithography to Millimeter and Infrared Devices," Proc. IEEE, 54, 657 (1966).

21. K. Ogawa, W. S. C. Chang, B. L. Sopori, and F. J. Rosenbaum, "A Theoretical Analysis of Etched Grating Coupler for Integrated Optics," Washington Univ. Tech. Report 72-5, AFOSR Contract F44-620-69-C-0121, St. Louis, May 1972.

22. D. Y. Tseng, "Equivalent Network Representation for High Efficiency Corrugated Blaze Grating," Appl. Optics (Sept. 1973).

23. H. Kogelnik and T. P. Sosnowski, "Holographic Thin Film Couplers," BSTJ 49, 1602 (1970).

24. H. Kogelnik, "Coupled Wave Theory for Thick Hologram Gratings," BSTJ 48, 2909 (1970).

25. W. J. Tomlinson and H. P. Weber, "Scattering Efficiency of High-periodicity Dielectric Gratings: Experiment," JOSA 63, 685 (1973).

26. J. C. Urbach and R. W. Meier, "Properties and Limitations of Hologram Recording Materials," Appl. Optics 8, 2269 (1969).

27. A. J. DeMaria, "Review of CW High-Power CO_2 Lasers," Proc. IEEE 61, 731 (1973).

APPENDIX A: OPTICAL DIELECTRIC WAVEGUIDES-- INFLUENCE OF INFRARED ACTIVE PHONONS IN THE WALL DIELECTRIC

by
J. D. McMullen

A. INTRODUCTION

An optical wave can propagate as a guided mode inside a capillary tube having dielectric walls.[1] Low-loss propagation occurs because of the high reflectivity of the dielectric wall for an optical wave at nearly grazing incidence. The propagation constant and losses of a straight dielectric capillary waveguide depend upon the ratio of free-space wavelength to tube diameter and upon the optical properties of both the inner core and the dielectric walls. Marcatilli and Schmeltzer pointed out that the propagation losses can be very small, so the capillary waveguide can be used for small bore diameter gas lasers.[2] Considerable experimental effort has been directed toward the construction of waveguide gas lasers because of their potentially high gain and pressure-broadened emission linewidth.

The purpose of this analysis is to examine the influence of absorption by phonons in the surrounding dielectric upon the propagation losses of the capillary waveguide mode. Previous calculations have been made of the effects of metallic and lossy dielectric walls at specific laser frequencies in the visible.[2,3] Abrams calculated the influence of the optical properties of sapphire, BeO, and fused silica upon the attenuation of the EH_{11} capillary mode between 900 cm^{-1} and 1200 cm^{-1} frequency.[4] However, for frequencies near a peak in reflectivity, the real refractive index can become sufficiently large so that the TE_{01} mode may have lower attenuation than the EH_{11} mode. Further, the ordinary and extraordinary dielectric functions used by Abrams can give only a qualitative indication of the frequency dependence of the mode attenuation since the EH_{11} mode can have no simple orientation of its electric field parallel or perpendicular to the $\hat{c}$ axis, particularly when the refractive index and the principal mode angle vary strongly with frequency.

When the emission lines of an infrared gas molecular laser lie near the transverse optical frequency of an infrared active phonon in the wall dielectric, the influence of the phonons upon the absorption and reflectivity of the walls causes the mode attenuation coefficient to vary rapidly with frequency. A case of current experimental interest is the CO_2 waveguide laser, using quartz, BeO or sapphire for the wall dielectric. The CO_2 emission lines between 9.2 and 10.6 microns lie near the absorption and reflectivity peaks for the TO phonons in these materials. The strong frequency dependence of the optical constants of the dielectric wall influence the mode attenuation of a small-bore tube over this frequency range.

In this paper the influence of phonon absorption in the wall dielectric is examined for the capillary optical waveguide between 100 cm^{-1} and 1200 cm^{-1} frequency for quartz, BeO and sapphire wall materials. The physical causes of structures in the frequency dependence of the mode attenuation coefficient are explained in terms of the influence of the transverse and longitudinal optical phonons on the optical properties of the dielectric.

B. THEORY

1. Capillary Waveguide Modes:

The analysis of the field distributions and propagation characteristics of the cylindrical dielectric waveguide have been given by Stratton.[1] Only the modes having lowest propagation loss are of interest for waveguide lasers. These modes correspond to near-grazing incidence of the wavefront with the wall, for which the reflectivity of the wall dielectric is very high. Marcatilli and Schmeltzer have shown that when the free-space wavelength λ is much smaller than the guide inner radius "a" and the electric field intensity varies slowly in the radial direction inside the core, the complex wave vector γ for a low-order capillary mode may be written as:

$$\gamma = \frac{2\pi}{\lambda}\left[1 - \frac{1}{2}\left(\frac{u_{nm}\lambda}{2\pi a}\right)^2\left(1 - \frac{i\lambda\nu_n}{\pi a}\right)\right] \qquad (1)$$

where u_{nm} is the root of the Bessel function $J_{n-1}(u_{nm})$ for the guided mode of order n,m. The mode parameter ν_n depends upon the dielectric properties of core and wall materials, and is given by:

$$\nu_n = \begin{cases} & |\epsilon(\omega) - 1|^{-1/2} & \text{for } TE_{om} \text{ modes} \\ \epsilon(\omega) & |\epsilon(\omega) - 1|^{-1/2} & \text{for } TM_{om} \text{ modes} \\ \frac{1}{2}|\epsilon(\omega) + 1| & |\epsilon(\omega) - 1|^{-1/2} & \text{for } EH_{nm} \text{ modes} \end{cases} \qquad (2)$$

The attenuation coefficient $1/L_G$ of the guided capillary mode is related to the imaginary part of the propagation constant γ.

There are two distinct physical causes for damping of a guided capillary mode:

(1) Refractive losses, and

(2) Absorption by the wall material.

Refractive losses correspond simply to refraction of the radiation into the higher-refractive-index wall dielectric, in accordance with Snell's law. Refractive losses depend upon the discontinuity in the real refractive index at the wall and upon the polarization of the electric field perpendicular or parallel to the plane of incidence with the wall.

The refractive losses of the lowest loss modes HE_{11} and TE_{01} are illustrated in Figure 1 as functions of the discontinuity in real refractive index at the wall. The attenuation coefficient α_{nm} (renormalized) of the HE_{11} mode is smaller for relative indices less than 2.02, and the TE_{01} mode attenuation is smaller for larger index discontinuities. The higher attenuation of the EH_{11} mode for larger refractive indices is caused by the increased proximity of the Brewster angle to the grazing incidence capillary mode angle, so that more of the wave polarized in the plane of incidence with the wall is refracted into the wall region.

Absorption losses occur because of the irreversible absorption of energy from the guided optical wave by infrared active phonons or free carriers in the surrounding material. Frequency dependent

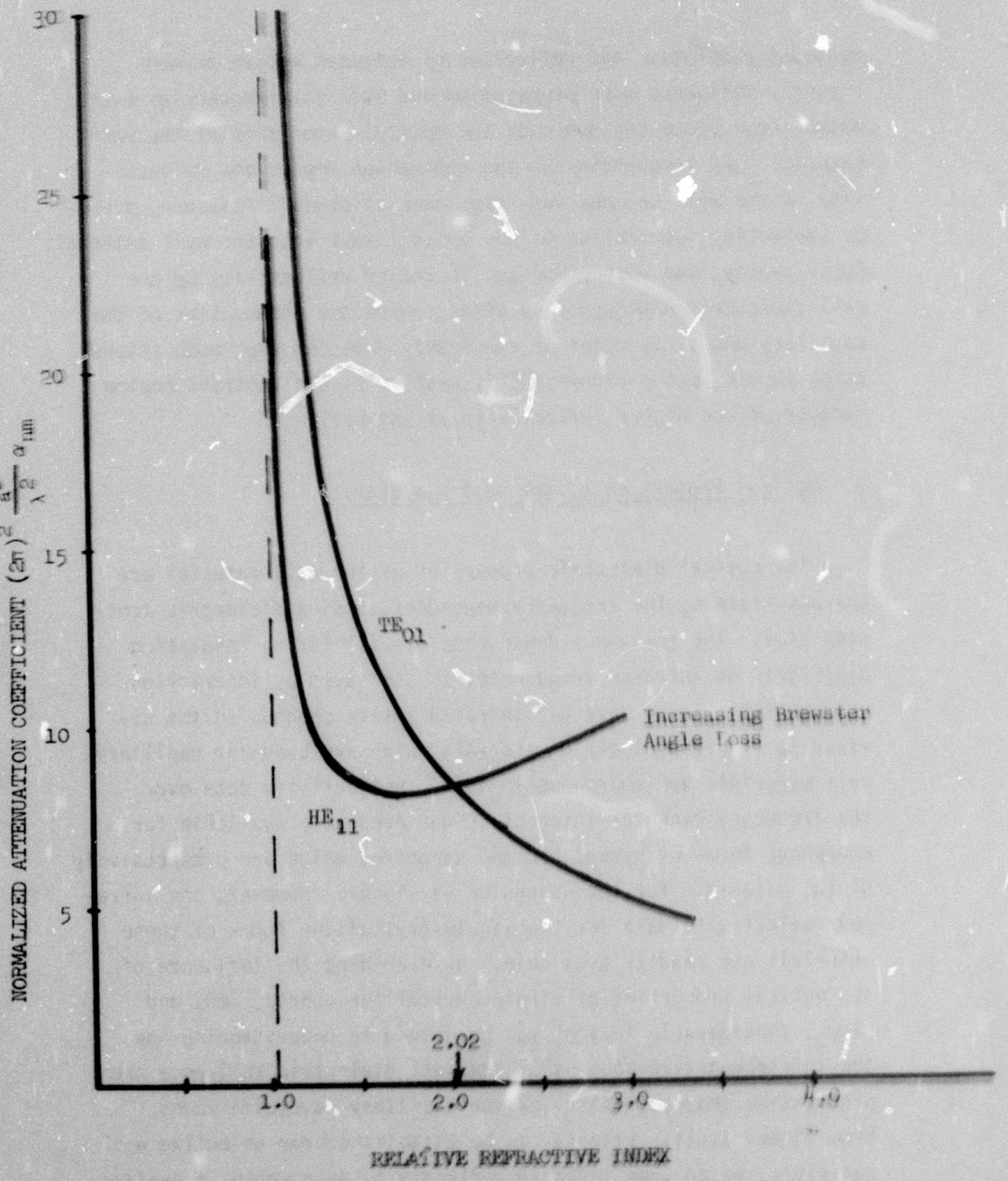

Figure 1. Attenuation of Capillary Waveguide TE_{01} and HE_{11} Modes as a function of the Relative Refractive Index between Core and Wall.

resonant absorption and reflection by infrared active phonons strongly influence mode propagation and loss for frequencies over which these processes dominate the optical properties of the wall material. At frequencies in the restrahlen regime the reflectivity of the wall becomes very high even at normal incidence, thereby preventing penetration of the optical wave into the wall material. Consequently, the absorption and increased reflectivity by the wall dielectric have opposite effects upon the attenuation of the capillary mode. It might be reasonably expected that mode attenuation should become significantly smaller in the restrahl regime because of the higher reflectivity at the wall.

2. Optical Properties of the Wall Dielectric:

The optical dielectric properties of the wall material are characterized by the frequency-dependent complex dielectric function $\epsilon(\omega)$. The frequency dependence of $\epsilon(\omega)$ for an insulating dielectric at infrared frequencies is dominated by interaction between the optical wave and infrared active phonons in the dielectric. Most dielectric materials which are used for capillary wall materials are amorphous in form. Reflectivity data over the frequency range of interest is not presently available for amorphous forms of pyrex, BeO and sapphire, which are prospectively useful materials for the waveguide gas laser. However, the infrared reflectivity data for the single-crystalline forms of these materials are readily available. By examining the influence of the optical properties of single-crystalline quartz, BeO, and Al_2O_3, considerable insight can be gained in understanding how the infrared active phonons of the wall dielectric influence the propagation characteristics of the capillary waveguide modes. From these results criteria can be established for selecting wall materials, based upon infrared reflectivity data which is available in the literature.

The ordinary and extraordinary dielectric functions $\epsilon(\omega)$ for a uniaxial crystal are given by:

Ordinary: $\epsilon_{\perp}(\omega)$ (3a)

Extraordinary: $\frac{1}{\epsilon_{\theta}(\omega)} = \frac{\cos^2\theta}{\epsilon_{\perp}(\omega)} + \frac{\sin^2\theta}{\epsilon_{//}(\omega)}$ (3b)

(3)

where θ is the angle between the wave vector $\underset{\sim}{k}$ and the $\hat{c}$ axis of the crystal, and $\epsilon_{\perp}(\omega)$ and $\epsilon_{//}(\omega)$ are the ordinary and extraordinary dielectric functions for electric fields polarized perpendicular to and parallel to the $\hat{c}$ axis, respectively. The dielectric functions for ordinary and extraordinary polarizations are given by:

$$\epsilon_{\perp}(\omega) = \epsilon_{\perp}(\infty) + \sum_{j=1}^{N_{\perp}} \frac{\epsilon_{\perp j}\omega_{\perp j}^2}{(\omega_{\perp j}^2 - \omega^2) - i\gamma_j\omega} \tag{4a}$$

$$\epsilon_{//}(\omega) = \epsilon_{//}(\infty) + \sum_{j=1}^{N_{//}} \frac{\epsilon_{// j}\omega_{// j}^2}{(\omega_{// j}^2 - \omega^2) - i\gamma_j\omega} \tag{4b}$$

(4)

There are $N_{\perp}$ infrared active phonon branches for $\underset{\sim}{E}$ perpendicular to $\hat{c}$ and $N_{//}$ branches for $\underset{\sim}{E}$ parallel to $\hat{c}$. ω_j, ϵ_j and γ_j are the resonant frequency, strength, and damping of each phonon branch. The high-frequency dielectric constant $\epsilon(\infty)$ for each polarization is measured at frequencies well above the lattice resonances and well below electronic resonances. The optical constants n and κ which describe wave propagation in the dielectric are defined in terms of the dielectric function by:

$$(n + i\kappa)^2 = \mathrm{Re}\ \epsilon(\omega) + i\mathrm{Im}\epsilon(\omega) \tag{5}$$

where n is the index of refraction and κ is the index of attenuation, commonly called the extinction coefficient. The attenuation coefficient 1/L for the intensity of radiation propagating through the dielectric is given by:

$$1/L = 4\pi\kappa/\lambda. \tag{6}$$

3. Influence of the Wall Dielectric Upon Mode Propagation:

In direct analogy to the case of propagation in a bulk crystal, a complex index of refraction may be defined for each capillary mode in terms of an effective mode refractive index N_G and extinction coefficient K_G. Propagation and attenuation of the waveguide mode are described by these coefficients, which are related to the complex wave vector γ of the mode:

$$\gamma = \frac{2\pi}{\lambda} (N_G + iK_G) \tag{7}$$

N_G and K_G give the phase velocity c/N_G of the mode and the rate of attenuation of the mode. The attenuation coefficient $1/L_G$ for the mode is given by:

$$1/L_G = 4\pi K_G/\lambda \quad . \tag{8}$$

where L_G is the distance the guided optical wave can propagate before decaying by a factor of 1/e in intensity.

4. Calculation of Mode Attenuation for Quartz, BeO and Sapphire Walls:

The extinction coefficient K_G for the TE_{01} circular electric capillary mode was calculated for quartz, BeO, and Al_2O_3 walls. For the cases studied, the tube bore is parallel to the c axis of the single-crystalline wall material, and the ordinary dielectric function $\epsilon_\perp(\omega)$ is used to describe the optical properties of the outer region. The parameters characterizing the ordinary dielectric function $\epsilon_\perp(\omega)$ for each material are listed in Tables I, II, and III, as given by previous infrared reflectivity and Raman experiments.[5-8]

The frequency dependence of the extinction coefficient K_G for the capillary mode is calculated from the imaginary part of the propagation constant γ. The frequency dependence of K_G is illustrated in Figures 2, 3, and 4 for wall materials of quartz (SiO_2), BeO, and sapphire (Al_2O_3), respectively. There is considerable

TABLE I

Infrared Dielectric Properties of Quartz*
For Ordinary Polarization $\underline{E} \perp \hat{c}$

Phonon Branch Index j	Transverse Optical Frequency ω_j (cm^{-1})	Dielectric Strength ϵ_j (no units)	Damping γ_j (cm^{-1})
1	394.	0.33	2.76
2	450.	0.82	4.05
3	697.	0.018	8.36
4	797.	0.11	8.07
5	1072.	0.67	7.61
6	1163.	0.01	6.98
7 (two-phonon)	1227.	0.009	134.97

*Reference 5 $\quad \epsilon_\perp(\infty) = 2.536$

TABLE II

Infrared Dielectric Properties of BeO*
For Ordinary Polarization $\underline{E} \perp \hat{c}$

$\omega_{TO} = 725.\ cm^{-1}$

$\epsilon_{Lattice} = 3.94$

$\gamma = 11.6\ cm^{-1}$

*Reference 6 $\quad \epsilon_\perp(\infty) = 2.95$

structure in the frequency dependence of the extinction coefficient K_G near the resonance frequencies of the infrared active optical phonons in the wall material. The extinction coefficient decreases by as much as a factor of 200 for frequencies between the TO and LO phonon frequencies. There are three prominent characteristics of the frequency dependence of K_G which may be related simply to the optical properties of the wall material:

TABLE III

Infrared Dielectric Properties of Sapphire*

For Ordinary Polarization $\underline{E} \perp \hat{c}$

Phonon Branch Index j	Transverse Optical Frequency $\omega_j (cm^{-1})$	Dielectric Strength ϵ_j (no units)	Damping γ_j (cm^{-1})
1	385.	0.3	5.87
2	442.	2.7	4.42
3	569.	3.0	11.38
4	635.	0.3	12.70

*References 7 and 8 $\epsilon_\perp(\omega) = 3.20$

(1) There is a sharp decrease in the extinction coefficient near the TO phonon frequency. The TO phonon frequency coincides with the abrupt drop on the low-frequency side of each minimum in K_G.

(2) The longitudinal optical (LO) phonon frequency defines the frequency just above the minimum in K_G at which the extinction coefficient begins to increase appreciably with frequency.

(3) There is a sharp, narrow peak in the mode extinction coefficient just above the LO phonon frequency.

The behavior of K_G at frequencies near and above the LO phonon frequency was at first a bit surprising, since the reflectivity for normal incidence upon the dielectric drops sharply with increasing frequency at the frequency of the LO phonon. The peak in the extinction coefficient K_G above the LO phonon frequency occurs at the frequency for which the real refractive index n

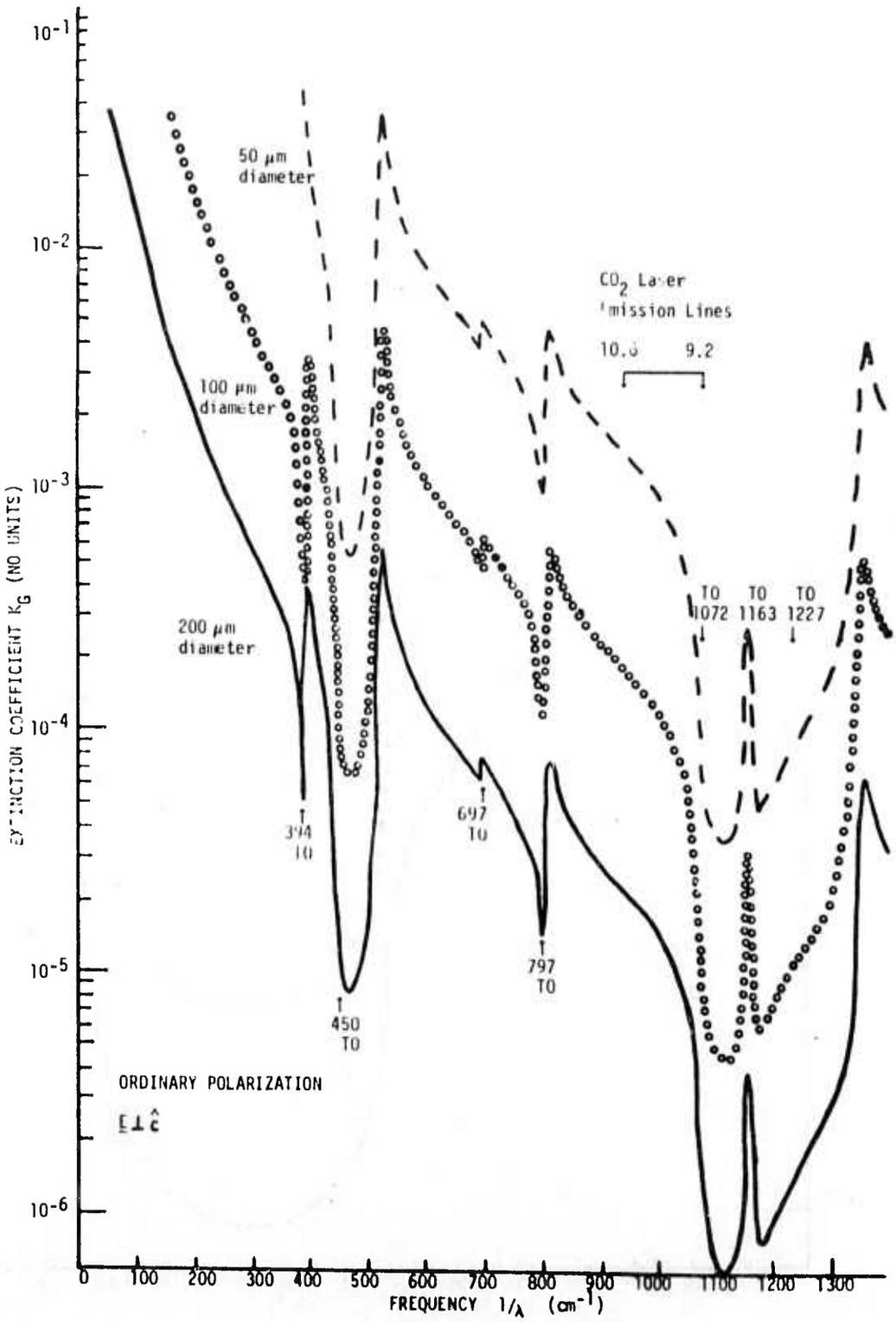

Figure 2. Frequency Dependence of the Extinction Coefficient for the TE_{01} Circular Mode of a Quartz Capillary Waveguide

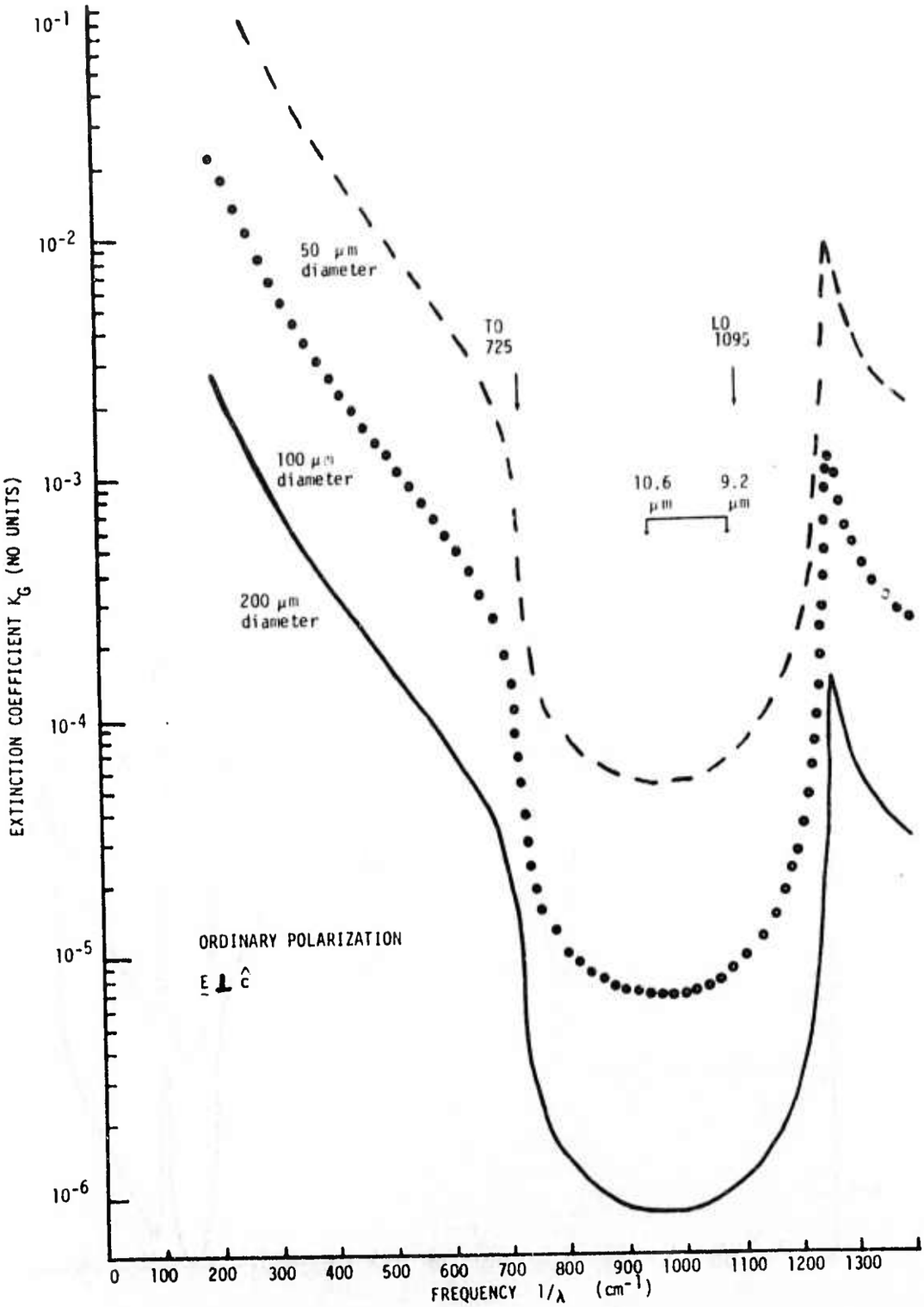

Figure 3. Frequency Dependence of the Extinction Coefficient for the TE_{01} Circular Mode of a BeO Capillary Waveguide

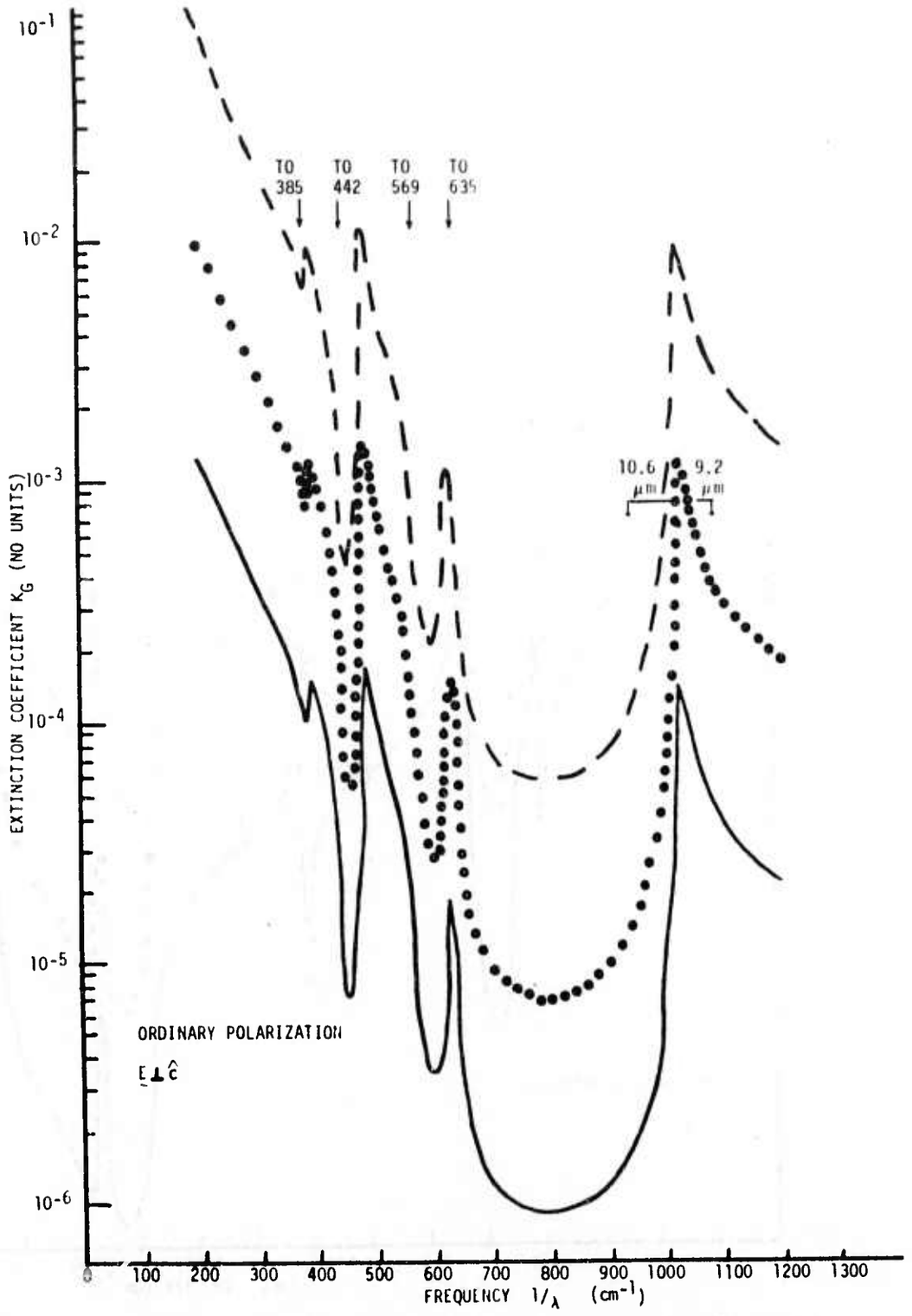

Figure 4. Frequency Dependence of the Extinction Coefficient for the TE_{01} Circular Mode of a Sapphire Capillary Waveguide

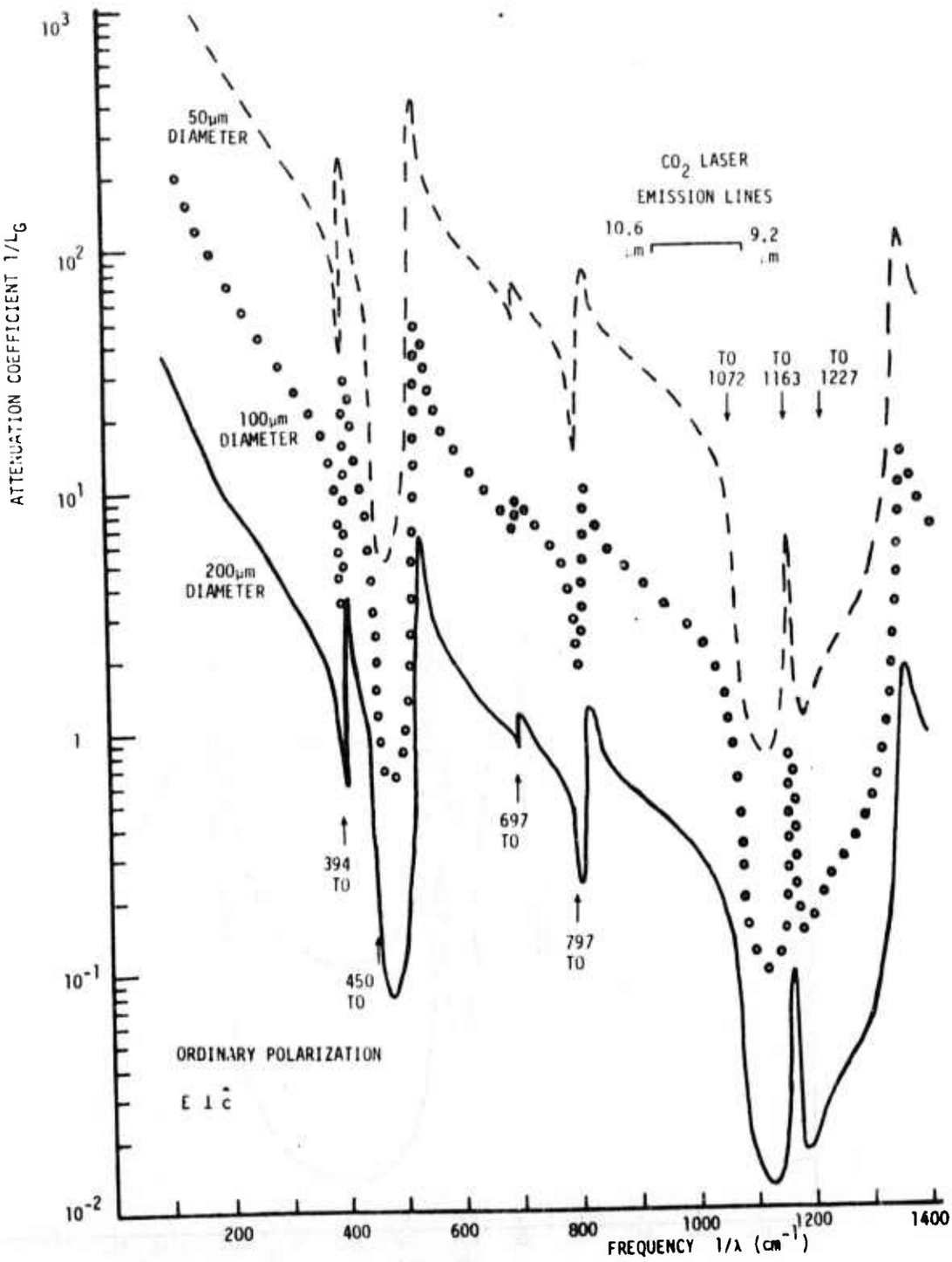

Figure 5. Frequency Dependence of the Attenuation Coefficient for the TE_{01} Mode of a Quartz Capillary Waveguide

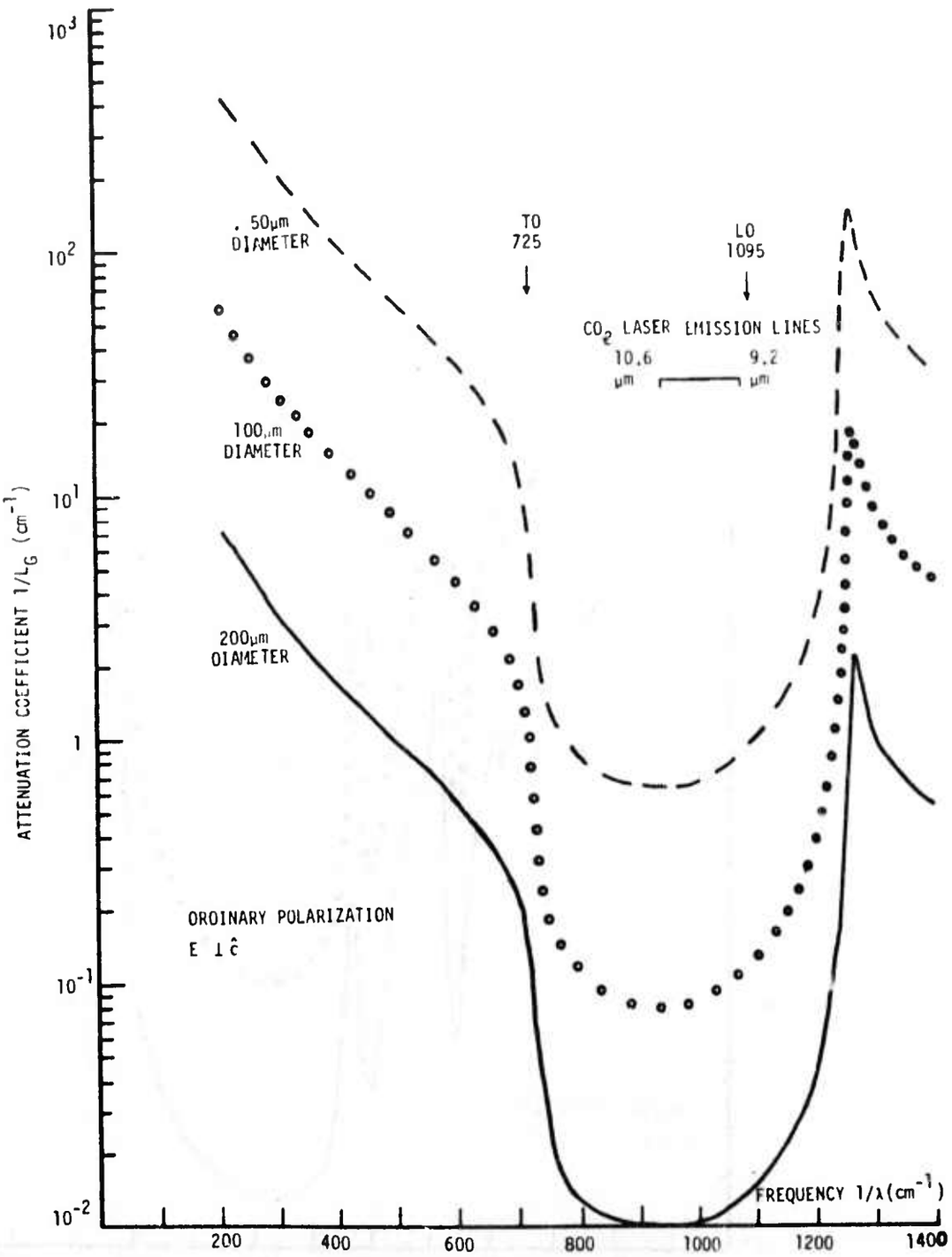

Figure 6. Frequency Dependence of the Attenuation Coefficient for the TE_{01} Mode of a BeO Capillary Waveguide

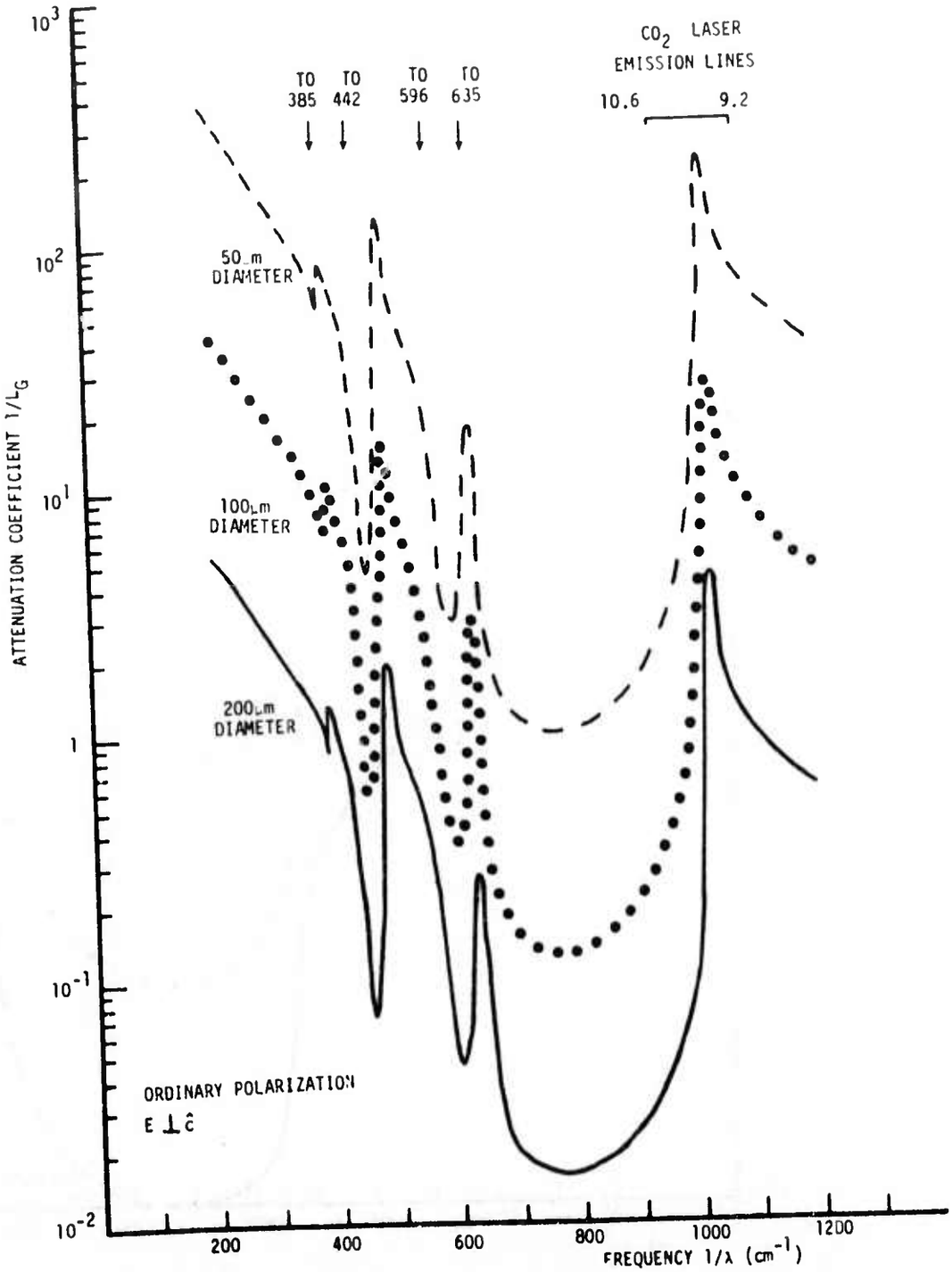

Figure 7. Frequency Dependence of the Attenuation Coefficient for the TE_{01} Mode of a Sapphire Capillary Waveguide

of the wall material is equal to the real refractive index in the core region. The attenuation index κ in the wall material is typically very small at this frequency. Refractive losses for the waveguide mode are very large at this frequency, since a discontinuity in refractive index does not exist in the values of the refractive indices at the wall. The three distinctive behaviors are most clearly demonstrated in Figure 3 for the ordinary polarization in a BeO capillary waveguide. The peak in K_G corresponding to $n = 1.0$, $\kappa = 0$ for the wall dielectric occurs at a frequency of 1260 cm^{-1}. When there are several phonon branches which are closely spaced in frequency, as for the higher frequency modes in quartz and sapphire, these separate effects are not always distinguishable.

The attenuation coefficient $1/L_G$ of the capillary mode is shown as a function of frequency in Figures 5, 6, and 7 for the three materials considered. In order to maintain a single-pass optical loss of less than one percent over a length of z cm, the mode attenuation $1/L_G$ must be less than $4.6/z$ cm^{-1}. For a 10-cm-long capillary laser, a tube bore greater than 70 microns in BeO will have acceptable optical loss. The minimum acceptable bore diameter in quartz is about 100 microns, and in sapphire 200 microns. Again, BeO is the most suitable material for a capillary laser operating between 9.2 and 10.6 microns, because of its high reflectivity between TO and LO phonon frequencies.

5. Criteria for Optimum Choice of Materials for Capillary Dielectric Waveguides:

A set of criteria is developed for evaluating the suitability of dielectric materials for capillary waveguides, based upon the optical properties of the dielectric. The data upon which the evaluation is based are readily available in the literature from infrared reflectivity and Raman experiments, or can be easily obtained by a reflectivity spectrum.

(1) The attenuation of the capillary waveguide mode is much smaller between the TO and LO phonon frequencies.

(2) The attenuation of the guided wave increases and peaks sharply at a frequency just above the LO phonon frequency, where the real refractive indices of the wall and core regions are equal.

The calculations which have been presented here are for the circular TE_{01} capillary mode. This mode exhibits the lowest attenuation in the restrahl region where the real refractive index becomes larger than 2.02. Calculations by Abrams and Bridges show qualitatively similar behavior in the frequency dependence of attenuation of the EH_{11} mode for BeO and sapphire.[4]

Of the three materials studied, the attenuation of the capillary mode is least for the case of BeO walls. However, in practice a polycrystalline pressed form of BeO is commonly used. The polished surface of this material contains a high density of pits when optically polished. Experimental measurements of mode attenuation may be significantly influenced by scattering from surface roughness if the pits are not much smaller than the optical wavelength.

6. Applicability of Results to the Case of the Planar Dielectric Waveguide:

The results of the calculations for the attenuation of the capillary waveguide mode can be extended qualitatively to the case of planar dielectric walls. The mechanism for wave-guiding is the same for both geometries, . . . specifically the high reflectivity of the dielectric for an optical wave at grazing incidence. The planar TM modes may be expected to have larger refractive losses for walls of large refractive index, because of "Brewster effect" enhancement of refraction into the outer regions. The attenuation coefficient for both TE and TM polarizations may be expected to drop sharply for frequencies between the TO and LO phonon frequencies in the wall dielectric. A peak in the attenuation of the capillary mode should occur just above the LO frequency, where the discontinuity in refractive index between core and wall becomes very small.